ornl

NUREG/CR-3982
ORNL-6099

OAK RIDGE
NATIONAL
LABORATORY

MARTIN MARIETTA

Case Study of the Propagation of a Small Flaw Under PWR Loading Conditions and Comparison with the ASME Code Design Life

Comparison of ASME Code Sections III and XI

G. T. Yahr
A. K. Richardson
R. C. Gwaltney
W. L. Server

Prepared for the U.S. Nuclear Regulatory Commission
Office of Nuclear Regulatory Research
Under Interagency Agreement DOE 40-550-75

8412190379 841130
PDR NUREG
CR-3982 R PDR

OPERATED BY
MARTIN MARIETTA ENERGY SYSTEMS, INC.
FOR THE UNITED STATES
DEPARTMENT OF ENERGY

NOTICE

Availability of Reference Materials Cited in NRC Publications

Most documents cited in NRC publications will be available from one of the following sources:

1. The NRC Public Document Room, 1717 H Street, N.W., Washington, DC 20555
2. The NRC/GPO Sales Program, U.S. Nuclear Regulatory Commission, Washington, DC 20555
3. The National Technical Information Service, Springfield, VA 22161

Although the listing that follows represents the majority of documents cited in NRC publications, it is not intended to be exhaustive.

Referenced documents available for inspection and copying for a fee from the NRC Public Document Room include NRC correspondence and internal NRC memoranda; NRC Office of Inspection and Enforcement bulletins, circulars, information notices, inspection and investigation notices; Licensee Event Reports; vendor reports and correspondence; Commission papers; and applicant and licensee documents and correspondence.

The following documents in the NUREG series are available for purchase from the NRC/GPO Sales Program: formal NRC staff and contractor reports, NRC-sponsored conference proceedings, and NRC booklets and brochures. Also available are Regulatory Guides, NRC regulations in the *Code of Federal Regulations*, and *Nuclear Regulatory Commission Issuances*.

Documents available from the National Technical Information Service include NUREG series reports and technical reports prepared by other federal agencies and reports prepared by the Atomic Energy Commission, forerunner agency to the Nuclear Regulatory Commission.

Documents available from public and special technical libraries include all open literature items, such as books, journal and periodical articles, and transactions. *Federal Register* notices, federal and state legislation, and congressional reports can usually be obtained from these libraries.

Documents such as theses, dissertations, foreign reports and translations, and non-NRC conference proceedings are available for purchase from the organization sponsoring the publication cited.

Single copies of NRC draft reports are available free, to the extent of supply, upon written request to the Division of Technical Information and Document Control, U.S. Nuclear Regulatory Commission, Washington, DC 20555.

Copies of industry codes and standards used in a substantive manner in the NRC regulatory process are maintained at the NRC Library, 7920 Norfolk Avenue, Bethesda, Maryland, and are available there for reference use by the public. Codes and standards are usually copyrighted and may be purchased from the originating organization or, if they are American National Standards, from the American National Standards Institute, 1430 Broadway, New York, NY 10018.

Notice

This report was prepared as an account of work sponsored by an agency of the United States Government. Neither the United States Government nor any agency thereof, nor any of their employees, makes any warranty, express or implied, or assumes any legal liability or responsibility for the accuracy, completeness, or usefulness of any information, apparatus, product, or process disclosed, or represents that its use would not infringe privately owned rights. Reference herein to any specific commercial product, process, or service by trade name, trademark, manufacturer, or otherwise, does not necessarily constitute or imply its endorsement, recommendation, or favoring by the United States Government or any agency thereof. The views and opinions of authors expressed herein do not necessarily state or reflect those of the United States Government or any agency thereof.

NUREG/CR-3982
ORNL-6099
Dist. Category RM

Engineering Technology Division

CASE STUDY OF THE PROPAGATION OF A SMALL FLAW UNDER PWR LOADING CONDITIONS AND COMPARISON WITH THE ASME CODE DESIGN LIFE

COMPARISON OF ASME CODE SECTIONS III AND XI

G. T. Yahr
A. K. Richardson
R. C. Gwaltney
W. L. Server

Manuscript Completed - October 3, 1984
Date Published - November 1984

Performed for the
U.S. Nuclear Regulatory Commission
Office of Nuclear Regulatory Research
Under DOE Interagency Agreement No. 40-550-75

NRC FIN Nos. B0474 and A6367

Prepared by the
OAK RIDGE NATIONAL LABORATORY
Oak Ridge, Tennessee 37831
operated by
MARTIN MARIETTA ENERGY SYSTEMS, INC.
for the
U.S. DEPARTMENT OF ENERGY
under Contract No. DE-AC05-840R21400

FOREWORD

The work reported here was performed at Idaho National Engineering Laboratory (INEL) and at Oak Ridge National Laboratory (ORNL). The work at INEL was sponsored by the U.S. Nuclear Regulatory Commission's (NRC's) ASME Code Section XI – Technical Support Program (FIN No. A6367), which is managed at INEL by W. L. Server. INEL is operated by EG&G Idaho, Inc., for the U.S. Department of Energy under Contract No. DE-AC07-76ID01570. The work at ORNL was sponsored by the U.S. NRC's ASME Code Section III – Technical Support Program (FIN No. B0474), which is managed at ORNL by G. T. Yahr. The original manager of both programs for the NRC, E. T. Baker, was succeeded by N. J. Miegel for FIN No. A6367 and D. J. Guzy for FIN No. B0474.

CONTENTS

	Page
LIST OF FIGURES	vii
LIST OF TABLES	ix
ACKNOWLEDGMENTS	xi
ABSTRACT	1
1. INTRODUCTION	1
2. PROBLEM DESCRIPTION	4
3. CODE SECT. III FATIGUE DESIGN APPROACH	9
3.1 Background	9
3.2 Results	11
4. FATIGUE CRACK-GROWTH ANALYSIS	19
4.1 Fatigue Crack-Growth Behavior	21
4.2 Section XI Analysis	22
4.3 Computer Code Analysis	23
4.4 Material Considerations	23
4.5 Thermal and Stress Analyses	25
4.6 Critical Flaw Size	27
4.7 Results of Crack-Growth Analyses	27
5. DISCUSSION	33
6. CONCLUSIONS	36
REFERENCES	38

LIST OF FIGURES

Figure		Page
1	ASME Code Sect. III high-cycle design fatigue curves for austenitic steels, nickel-chromium-iron alloy, nickel-iron-chromium alloy, and nickel-copper alloy for temperatures not exceeding 800°F	10
2	Relationship between maximum postulated defect and allowable surface indications	20
3	Relationship between surface and subsurface reference flaws	20
4	Permissible surface flaw size limits and allowable indication standards vs flaw aspect ratio	21
5	Compiled fatigue crack-growth data for 316 stainless steel	24
6	Axial stress distribution through the pipe wall as function of time for step increase/decrease, Transients e, f	26
7	Crack depth determined using Sect. XI analysis as function of 40-year design lifetimes and usage factor ...	30

LIST OF TABLES

Table		Page
1	Zion-1 events	5
2	Load transients for hot-leg pipe based on Zion-1	6
3	Maximum stress components caused by individual transients	6
4	Stress ranges	7
5	Unit histograms for Zion-1	8
6	Derivation of loads in Zion-1 hot-leg piping	12
7	Tabulated stress used in Eqs. (1) and (2)	14
8	Stress indices used in fatigue stress calculations	15
9	Section III fatigue analysis results for straight pipe with fatigue strength reduction factors all equal to 1.0	15
10	Section III fatigue analysis results for flush weld	16
11	Section III fatigue analysis results for as-welded condition	16
12	Section III fatigue analysis results using highest possible stress concentration	17
13	Section III fatigue analysis results using stress concentration factor for crack	17
14	Section III fatigue analysis results using stress concentration for crack and flush weld in combination	18
15	Number of lifetimes required to produce usage factor of 1.0	18
16	Section XI analyses of Sect. III allowable flaw for 40-year design lifetime	28
17	Number of 40-year lifetimes until critical flaw size for Sect. III allowable flaw	28

Table		Page
18	Section XI analyses of Sect. XI allowable preservice flaw for 40-year design lifetime	29
19	Number of 40-year lifetimes until critical flaw size for Sect. XI allowable preservice flaw	29
20	Computer code DRIVE analysis for Sect. III allowable flaw for 40-year design lifetime	32
21	Crack computer code DRIVE analyses for Sect. XI allowable preservice flaw for 40-year design lifetime	32

ACKNOWLEDGMENTS

The authors wish to acknowledge the contributions of C. J. Pientka of EG&G Idaho, who assisted with the computer code DRIVE, and B. L. Harris and K. H. Liebelt of EG&G Idaho, who conducted the thermal and stress analyses.

Thanks are also due to the Metal Properties Council Task Force on Crack Propagation Technology (D. P. Jones, chairman); the American Society of Mechanical Engineers (ASME) Subgroup on Fatigue Strength (W. J. O'Donnell, chairman); the ASME Sect. XI Subgroup on Evaluation Standards (S. Bush, chairman); and W. H. Cullen, R. R. Maccary, S. W. Tagart, C. R. Brinkman J. G. Merkle, G. H. Weidenhamer, and F. Hill for their comments and assistance. Finally, we acknowledge the support and encouragement of W. F. Anderson, E. T. Baker, D. J. Guzy, and N. Miegel.

CASE STUDY OF THE PROPAGATION OF A SMALL FLAW UNDER PWR LOADING CONDITIONS AND COMPARISON WITH THE ASME CODE DESIGN LIFE

COMPARISON OF ASME CODE SECTIONS III AND XI

G. T. Yahr
A. K. Richardson*
R. C. Gwaltney
W. L. Server*

ABSTRACT

A cooperative study was performed by EG&G Idaho, Inc., and Oak Ridge National Laboratory to investigate the degree of conservatism and consistency in the *ASME Boiler and Pressure Vessel Code* Sect. III fatigue evaluation procedure and Sect. XI flaw acceptance standards. A single, realistic, sample problem was analyzed to determine the significance of certain points of criticism made of an earlier parametric study by staff members of the Division of Engineering Standards of the Nuclear Regulatory Commission. The problem was based on a semielliptical flaw located on the inside surface of the hot-leg piping at the reactor vessel safe-end weld for the Zion 1 pressurized-water reactor (PWR). Two main criteria were used in selecting the problem; first, it should be a straight pipe to minimize the computational expense; second, it should exhibit as high a cumulative usage factor as possible. Although the problem selected has one of the highest cumulative usage factors of any straight pipe in the primary system of PWRs, it is still very low.

The Code Sect. III fatigue usage factor was only 0.00046, assuming it was in the as-welded condition, and fatigue crack-growth analyses predicted negligible crack growth during the 40-year design life. When the analyses were extended past the design life, the usage factor was less than 1.0 when the flaw had propagated to failure. The current study shows that the criticism of the earlier report should not detract from the conclusion that if a component experiences a high level of cyclic stress corresponding to a fatigue usage factor near 1.0, very small cracks can propagate to unacceptable sizes.

---

1. INTRODUCTION

The fatigue design approach of Sect. III of the *ASME Boiler and Pressure Vessel Code*[1] is based on the experimentally determined relationship between elastically calculated stress range and fatigue life.[2] Fatigue damage accumulated by the component at different stress ranges is

---

*EG&G Idaho, Inc., Idaho Falls, Idaho.

accounted for by linearly adding the fraction of life consumed at each stress range. This cumulative usage factor is not allowed to exceed unity.

Section XI of the *ASME Boiler and Pressure Vessel Code*[3] includes a procedure that allows continued operation after defects are found during inservice inspection by using a fatigue crack-growth analysis to demonstrate that the defect will not propagate to a critical size prior to the next inspection. Because this procedure is, in essence, a fundamentally different fatigue design approach from the cumulative usage factor approach of Sect. III, it is natural that the consistency of the two approaches, which will actually be applied to the same component, would be questioned. More importantly, indications of possible defects below certain sizes are not a cause for rejection under Sect. III. Section XI allows defects of certain sizes without requiring reanalysis. A logical question that arises is whether those acceptable defect indications always meet the requirements of Sect. XI when they are found after the component has been placed in service.

In NUREG-0726 (Ref. 4), a simplified analysis was done to calculate the magnitude of acceptable crack sizes consistent with the maximum fatigue usage allowed by the ASME Code. This analysis indicated that if a component experiences a high level of cyclic stress corresponding to a usage factor of 1.0, very small cracks can propagate to sizes that exceed acceptance criteria. This work received considerable criticism by industry. The principal criticisms were concerned with the simplifications employed in the analysis, which were recognized by the authors when the analysis was done.

As a result of the work reported in Ref. 4, staff members in the Division of Engineering Standards [now identified as the Division of Engineering Technology (DET)] of the Nuclear Regulatory Commission (NRC) became concerned about the consistency and relationship between the fatigue design curves in Sect. III, crack-growth curves in Sect. XI, and the defect acceptance standards in Sects. III and XI of the *ASME Boiler and Pressure Vessel Code*. Therefore, the present study was initiated to determine whether these concerns are justified and whether some restrictions may be necessary when predicting the fatigue life of a flawed component. The present study was not designed to be a sufficient basis for recommending Code changes; it was intended to determine the validity of specific points of criticism of the earlier study by examining a realistic component.

The fatigue rules for Class 1 components in Sect. III of the ASME Code use S-N curves derived from data that were obtained from polished 1/4-in.-diam specimens and Miner's linear damage hypothesis. The flaw evaluation procedures of Sect. XI of the Code use linear-elastic fracture mechanics (LEFM) to predict the growth of existing flaws under cycling loading. Undetectable flaws and manufacturing defects sometimes exist in components. It is reasonable to suppose that such cracklike defects will propagate under cyclic loading if the stress range is high enough. For consistency, use of the Sect. XI LEFM procedures should not predict crack growth of expected flaws to critical size when the rules of Sect. III are satisfied. However, the simple and preliminary analyses of NUREG-0726 indicate that very small cracks can propagate to sizes that exceed the critical flaw size and cause failure if the crack area experiences a

usage factor close to unity. Thus, there is concern that the fatigue design requirements of Sect. III and the crack acceptance standards of Sect. XI might need to be changed. Therefore, a more detailed study was undertaken to determine whether changes are needed in Sects. III and XI to ensure conservatism and consistency.

2. PROBLEM DESCRIPTION

An actual reactor component was analyzed to ensure that the conclusions of NUREG-0726 (Ref. 4) are relevant because much of the criticism was that a realistic load histogram was not used. A simple geometry was chosen to avoid unnecessary analytical complexity. Furthermore, the problem was selected on the basis of having a relatively high usage factor. The highest usage factor in the primary coolant system of a pressurized-water reactor (PWR) is generally at the terminal end of the hot-leg pipe. Usage factors as high as 0.95 have been calculated at that location,[5] and the problem was selected on the basis of that reference. Although it was later discovered that current designs result in much lower usage factors at this location, the study was continued because higher usage factors were found only in complex geometries such as nozzles and elbows of PWR primary systems.

The plant chosen to serve as the basis for the present study is Westinghouse's PWR Zion-1 reactor. This particular plant was chosen because necessary information on loading, including thermal transients, is available in the open literature[6,7] and because the pipe is not clad. The location is the terminal end of the hot-leg piping where it is welded to the "safe end," which is attached to the outlet nozzle of the reactor vessel. The nominal inside diameter of the pipe is 29 in., and the nominal wall thickness is 2.5 in. The hot-leg pipe was manufactured out of SA-376 type 316 stainless steel material.

To evaluate the conservatism of Sect. XI acceptance standards, an analysis of fatigue crack-growth effects on a defect that was just acceptable by both the Sects. III and XI standards was desired. Since the DET wanted potentially the worst case, a surface flaw was chosen because of the higher stress-intensity factor for the same size flaw. Section III acceptance limits [NB-2540 (Ref. 8)] allow surface linear indications with dimensions less than 3/16 in. and internal elongated indications of 3/4-in. length for thicknesses greater than 2-1/4 in. The size of this surface indication is so small that any flaw depth with an aspect ratio less than 0.5 is easily acceptable under Sect. XI (IWB-3514). Therefore, two approaches to a flaw model were used.

1. The first approach (which was chosen by the DET as the overall model to be used) uses the 3/16-in. length specified in Sect. III for actual surface linear indications. A flaw depth of 0.050 in. was chosen based upon a radiography detection limit of a depth of 2% of the wall thickness. The corresponding aspect ratio a/ℓ, of 0.267, is consistent with the aspect ratios of flaws generally found in service.[9] If the eventual crack-growth analyses prove conservative, this particular flaw will not prove anything meaningful about the Sect. XI acceptance limits.

2. The other approach uses the Sect. XI flaw characterization approach that treats an internal (subsurface) indication near the surface as if it were a surface flaw. It is assumed that crack growth will immediately cause an internal defect to penetrate to the surface. Using the 3/4-in. allowable length ℓ from Sect. III for an internal indication, critical defect depths can be determined by use of the ASME Sect. XI acceptance standards for preservice and inservice inspection (Table IWB-3514-2). Flaw aspect ratios a/ℓ of 0.288 and 0.366 are obtained,

dictating depths of 0.216 and 0.2745 in. for preservice and inservice inspection, respectively.

The service loads for Zion-1 were obtained from Refs. 6 and 7. Vibration loading is not normally included in the service loads considered in the fatigue evaluation of PWR components and was not included in the service loads considered in Refs. 6 and 7. A study of PWR cold-leg piping integrity at Battelle Columbus Laboratories[10] showed that vibration loading could make an important contribution to fatigue crack growth. In the absence of appropriate data on levels of vibration of the hot legs in PWRs, the values assumed by the Battelle investigators for vibration in the cold legs of PWRs were also assumed in the present study. The assumed vibration stress variation of 1000-psi range at a frequency of 1000 cycles/min could result from pipe vibrations caused by such things as flow-induced vibration. The events considered and the number of times they occur are given in Table 1. The loads during each transient are given in Table 2. The maximum stress components at the inside and outside surfaces are given for each transient in Table 3. The stress ranges are given in Table 4, and the unit histograms are given in Table 5. The selection of the unit histograms is critical to a crack propagation analysis. Extreme cycles early in the histogram may propagate the crack sufficiently so that subsequent moderate cycles will cause additional crack propagation. If those same moderate cycles had been applied first, the crack would have propagated less. Standard histograms have been developed in the aerospace industry based on many years of flight data, but this concept has not been developed for nuclear plants. The unit histograms in Table 5 were arrived at by uniformly distributing all transients over the plant life. Because all the postulated cycles for the various transients are not convenient, even, multiples of the startup/shutdown transient, it was necessary to devise a method to distribute the "odd" transients uniformly during the plant life. Therefore,

Table 1. Zion-1 events

Transient	Event	Number of events
a, b	Startup/shutdown	500
c, d	Plant loading/plant unloading	15,000
e, f	Step increase/step decrease	2,000
g	Reactor trip and recover at startup	400
l	Loss of flow and abnormal loss of load	80
m	Loss of secondary pressure	5
h	Hydrotest to 3125 psig, 400°F	10
OBE	Operating basis earthquake	200
SSE	Safe shutdown earthquake	1
Vib.	Vibrations	2.1×10^{10}

Table 2. Load transients for hot-leg pipe based on Zion-1

Transient	Pressure (psig)	Bending moment[a] (in.-lb)	Delta temperature through wall (°F)
a, b	2235	1.22×10^7	19
c, d	110	(50/480)	24
e, f	220	(20/480)	12
g	510	(90/480)	117
l	550	(120/480)	190
m	2235	(301/480)	410
h	3125	(330/480)	19
OBE		2.77×10^7	
SSE		2.82×10^7	

[a]Source of moments — Startup/shutdown: This is for a temperature change from 70 to 550°F. For other transients, a fraction of this is used based on the ratio of temperature changes in the transients to 480°F (e.g., Transient c, d).

Table 3. Maximum stress components caused by individual transients

Transient	Axial stress (ksi)		Hoop stress (ksi)		Number of cycles
	In	Out	In	Out	
a, b	18.03	20.55	16.42	18.65	500
c, d	5.14	5.27	4.98	5.09	15,000
e, f	3.09	3.24	3.49	3.71	2,000
g	23.87	24.30	24.28	24.77	400
l	37.63	38.16	37.80	38.32	80
m	84.93	86.28	87.75	89.98	5
h	18.83	21.49	21.57	24.70	10
OBE	13.05	15.26			200
SSE	13.22	15.50			1
Vib.	1.0	1.0	1.0	1.0	2.1×10^{10}

Table 4. Stress ranges[a]

Transient	Axial stress (ksi)				Hoop stress (ksi)			
	Inside		Outside		Inside		Outside	
	Maximum	Minimum	Maximum	Minimum	Maximum	Minimum	Maximum	Minimum
a, b	18.03	0.0	20.55	0.0	16.42	0.0	18.65	0.0
c, d	23.17	17.71	25.82	20.18	21.40	15.78	23.74	17.90
e, f	21.12	17.39	23.79	19.80	19.91	15.14	22.36	17.15
g	40.42	16.55	43.12	18.83	37.74	13.46	39.97	15.20
l	55.66	16.44	58.71	18.68	54.22	13.23	57.07	14.91
m	96.48	11.55	99.23	12.95	91.20	3.45	93.43	3.45
OBE	31.08	4.98	35.81	5.29				
SSE	31.25	4.81	36.05	5.05				
Vib.[b]	19.03	17.03	21.55	19.55	17.42	15.42	19.65	17.65

[a] NOTE: The approach taken in the development of the stress ranges is based on the assumption that, with the exception of the hydrostatic test, all transients occur during the steady state operation. Thus the combination of stress ranges to form a stress cycle has been performed with regard to the startup/shutdown stress cycle. The maximum stress for the startup/shutdown cycle has been termed the steady state stress.

Pressure stress range

The following pressure transients have been treated as symmetric oscillations about the steady state pressure stress: (1) plant loading/plant unloading, (2) step increase/step decrease, and (3) loss of flow and abnormal loss of load. The following pressure transients have been treated as a steady decrease in the pressure stress from the steady state: (1) reactor trip and recover at startup, and (2) loss of secondary pressure. The hydrostatic test has been treated as if the pressure rose from zero to the test pressure.

Moment stress ranges

All bending moment stresses were treated as increasing from steady state.

Thermal gradient stress ranges

All thermal gradient stresses were treated as increasing from steady state.

[b] Estimated value NUREG/CR-2189.

Table 5. Unit histograms for Zion-1

Block No.	Transient	Number of cycles
1	a, b	1
	e, f	4
	c, d	30
	g	1
	Vibration	4.2×10^7
2	a, b	1
	h	2
	OBE	40
	l	16
	m	1
	e, f	4
	c, d	30
	g	1
	Vibration	4.2×10^7
3	SSE	1

Block No.	Number of repeats
1	99
2	1
1	99
2	1
1	99
2	1
1	99
2	1
1	99
2	1
3	1

the three different blocks were devised to simplify the computations. The first block included only the five most frequent events; the second included those plus five other less frequent events; and the third included only the Safe Shutdown Earthquake (SSE). This same approach was used in the cold-leg integrity evaluation at Battelle.[10]

3. CODE SECTION III FATIGUE DESIGN APPROACH

3.1 Background

The fatigue design approach of Sect. III (Refs. 1, 11, 12) of the *ASME Boiler and Pressure Vessel Code* for less than 10^6 cycles is based on concepts developed by Langer[2] on the basis of the Manson-Coffin[13,14] relationship between plastic strain amplitude and fatigue life. The relationship between plastic strain amplitude and fatigue life has been established by extensive strain-control push-pull fatigue testing of smooth 1/4-in.-diam, unflawed, hourglass-shape specimens. The design curves of ASME Code Sect. III are based on a best-fit curve drawn through the test data that has been lowered by a factor of either 2 on stress or 20 on cycles, whichever is more conservative at each point. At cyclic lives below about 4×10^3 cycles, the factor of 20 on cycles is the controlling factor so that the factor of safety on stress in this low-cycle regime is more than 2. At cyclic lives above about 4×10^4 cycles, the factor of 2 on stress is the controlling factor and the factor of safety on cyclic life is more than 20.

Reference 15 cites five specific things that are accounted for by the factor of 2 on stress: surface finish, size, material variability, environment, and residual stress. Other things that are not accounted for by the factor of 2 on stress, which must therefore be allowed for in the design and analysis, include stress concentration, corrosion, and metallurgical notch effects caused by differences in the weld and base metal.

Tests[11,16] on prototypic welded pressure vessels and piping with girth butt welds[17] have generally demonstrated that the design curves obtained using the factors of 2 and 20 are adequate. Some of the tests on 6-in. pipes with girth butt welds[18] included welds that had an intentional defect, that is, a lack of penetration produced by not completing a 1-in. section of root pass. Although their lives were less than those of similar pipes without intentional defects, their lives were longer than predicted by the Code Sect. III fatigue design procedure.

A large number of fatigue tests were carried out by Harrison and Maddox[19] on near full-size pressure vessels. Harrison and Maddox compared the results from these tests with fatigue design curves of the ASME Code Sects. III and VIII and the *British Vessel Code* BS-5500. Comparisons between the design curves and the test results were made for the following regions: at the toes of nozzle welds, at nozzle welds failing under circumferential stress loading, in the main seam welds, in repair welds, and in parent metal. In each of these regions, failures occurred below the S-N curves given in the ASME Code and, in some cases, below the S-N curves given in BS-5500.*

---

*These results have drawn a reaction from the ASME Code Committee; it has drafted a letter to Dr. Harrison citing two basic errors in Harrison and Maddox's application of the ASME Code rules. The letter states that correct evaluation of the data will show the Code rules to be significantly more conservative than the paper indicates.

The fatigue curves of ASME Code Sect. III are logarithmic plots of stress-intensity amplitude S vs number of cycles to failure N. The experimental data were actually based on strain-control tests, and the stress values used for plotting the data were determined by multiplying by the modulus of elasticity. The actual stresses were considerably lower than these fictitious stresses in the low-cycle regime ($<10^4$ cycles) where considerable plasticity occurs. However, this fictitious stress has the advantage of being directly comparable to elastically calculated stresses.

More recently, the high-cycle regime has received increased attention,[20,21] and the fatigue curves for austenitic stainless steel that previously stopped at 10^6 cycles have been extended to 10^{11} cycles. Because of the need to distinguish between load-controlled and strain-controlled cycling and to account for mean stress effects in the very high cycle regime, three curves are provided in the Code for fatigue design for lives above 10^6 cycles and are shown in Fig. 1 (Refs. 15, 22). Curve A is an extension of the low-cycle Code S-N curve for $<10^6$ cycles using the original Langer equation. Curve B corresponds to the original fatigue design curve at 10^6 cycles and to one-half of the average fatigue stress amplitude for annealed stainless steel under load-controlled cycling beyond 10^7 cycles.[23] Curve C was obtained from the stress-controlled data curve adjusted for the maximum effect of mean stresses that can be retained during cycling. A flow chart is given in the Code for determining which of the three curves should be used.

Miner's linear damage theory[24] is used for determining the cumulative damage from different load cycles. A fatigue usage factor is calculated by summing the ratios of the number of cycles expected to the number of allowable cycles determined from the S-N curve for all the stress cycles that are postulated to occur. The fatigue damage is taken

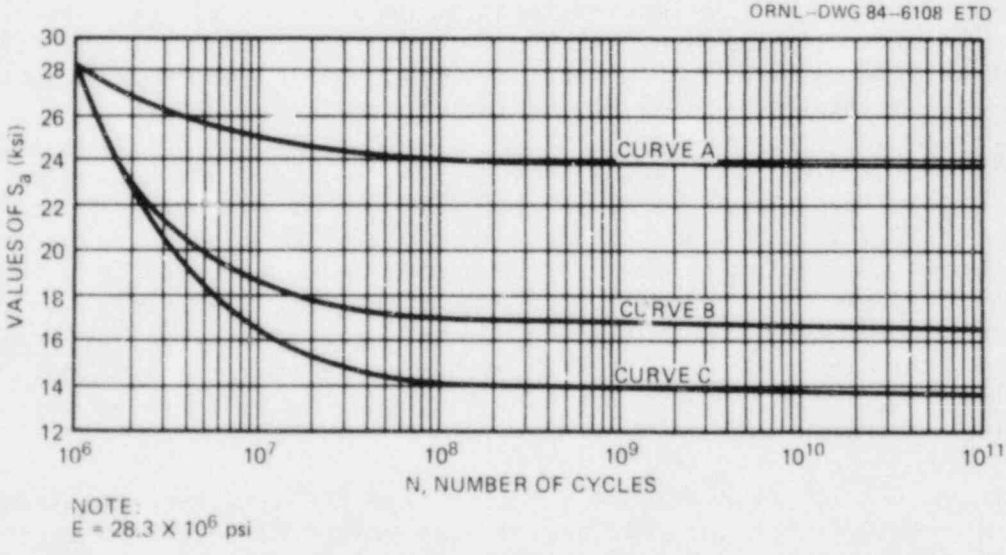

Fig. 1. ASME Code Sect. III high-cycle design fatigue curves for austenitic steels, nickel-chromium-iron alloy, nickel-iron-chromium alloy, and nickel-copper alloy for temperatures not exceeding 800°F (from Ref. 22).

as zero for stress cycles that are less than the allowable stress at 10^{11} cycles. Rodabaugh and Wright[25] have demonstrated the application of the Code Sect. III fatigue evaluation procedures to nuclear piping systems.

3.2 Results

Loads and stress ranges were derived for the terminal end of the Zion-1 hot-leg piping on the basis of the data in Refs. 6 and 7 and are given in Table 6. The thermal stresses in Table 6 are based on the temperature distributions given in Ref. 26.

The fatigue evaluation procedure used is given in Sect. III of the Code.[27] Equations (10) and (11) of Ref. 27 were used in the fatigue analysis of the hot-leg pipe. Equation (10) of Ref. 27 is

$$S_n = C_1 \frac{P_o D_o}{2t} + C_2 \frac{D_o}{2I} M_i + C_3 E_{ab} \times |\alpha_a T_a - \alpha_b T_b| \leq 3 S_m , \qquad (1)$$

where

$\alpha_a(\alpha_b)$ = coefficient of thermal expansion on side a(b) of a gross structural discontinuity or material discontinuity, at room temperature, 1/°F (Table I-5.0);
D_o = outside diameter of pipe, in.;
E_{ab} = average modulus of elasticity of the two sides of a gross structural discontinuity or material discontinuity at room temperature, psi (Table I-6.0);
t = nominal wall thickness of product, in.;
I = moment of inertia, in.^{4} (NB-3683);
C_1, C_2, C_3 = secondary stress indices;
M_i = resultant range of moment that occurs when the system goes from one service load set to another;
P_o = range of service pressure, psi;
$T_a(T_b)$ = range of average temperature on side a(b) of gross structural discontinuity or material discontinuity, °F;
S_m = allowable design stress intensity value.

This equation calculates the primary plus secondary stress-intensity range and must be less than three times the allowable design stress-intensity values ($<3 S_m$) to be valid. All load sets met this requirement because they were less than the $3 S_m$ value for this problem of 51 ksi. Equation (11) of Ref. 27 is

$$S_p = K_1 C_1 \frac{P_o D_o}{2t} + K_2 C_2 \frac{D_o}{2I} M_i + \frac{1}{2(1-\nu)} K_3 E\alpha |\Delta T_1| + K_3 C_3 E_{ab}$$

$$\times |\alpha_a T_a - \alpha_b T_b| + \frac{1}{1-\nu} E\alpha |\Delta T_2| , \qquad (2)$$

Table 6. Derivation of loads in Zion-1 hot-leg piping

Transient	Load range	Axial stress (ksi)		Hoop stress (ksi)		Project specification cycles
		In	Out	In	Out	
Startup/shutdown	P = 2235 psi	6.48	7.6	12.97	15.2	500
	M_B = 1.21699 × 10^7 in.-lb	5.71	6.7			
	ΔT = 19°F	3.45	3.45	3.45	3.45	
	M_W = 5.08591 × 10^6 in.-lb	2.39	2.8			
	Total	18.03	20.55	16.45	18.65	
Plant loading/plant unloading	P = 110 psi	0.32	0.37	0.64	0.75	15,000
	M_B = (50/480)	0.48	0.56			
	ΔT = 24°F	4.34	4.34	4.34	4.34	
	Total	5.14	5.27	4.98	5.09	
Step increase/step decrease	P = 220 ps'	0.64	0.75	1.28	1.50	2,000
	M_B = (20/480)	0.24	0.28			
	ΔT = 12°F	2.21	2.21	2.21	2.21	
	Total	3.09	3.24	3.49	3.71	
Reactor trip/ recover at startup	P = 510 psi	1.48	1.73	2.96	3.45	400
	M_B = (90/480)	1.07	1.25			
	ΔT = 117°F	21.32	21.32	21.32	21.32	
	Total	23.87	24.30	24.28	24.77	
Loss of flow/ abnormal loss of load	P = 550 psi	1.59	1.87	3.19	3.74	80
	M_B = (120/480)	1.43	1.68			
	ΔT = 190°F	34.61	34.61	34.61	34.61	
	Total	37.63	38.16	37.80	38.32	
Loss of secondary pressure	P = 2235 psi	6.48	7.6	12.97	15.2	5
	M_B = (301/480)	3.58	4.20			
	ΔT = 410°F	74.87	74.78	74.78	74.78	
	Total	84.93	86.28	87.75	89.98	
Hydrotest to 3125 psig, 400°F	P = 3125 psi	9.06	10.63	18.12	21.25	10
	M_B = (330/480)	3.93	4.61			
	ΔT = 19°F	3.45	3.45	3.45	3.45	
	M_W = 5.08591 × 10^6 in.-lb	2.39	2.8			
	Total	18.83	21.49	21.57	24.70	
Vibration		1.0	1.0	1.0	1.0	2.1 × 10^{10}
OBE	M_B = 2.77182 × 10^7 in.-lb	13.05	15.26			200
SSE	M_B = 2.81541 × 10^7 in.-lb	13.22	15.5[a]			1
Normal plant variations	P = ±50 psi	0.15	0.17	0.29	0.34	10^6
	ΔT = ±6°F	1.09	1.09	1.09	1.09	
	Total	1.24	1.26	1.38	1.43	

[a]Combined nonseismic and SSE stresses; SSE stress = 0.485 ksi.

where

K_1, K_2, K_3 = local stress indices;
$|\Delta T_2|$ = absolute value of the range for that portion of the nonlinear thermal gradient through-the-wall thickness not included in ΔT_1 as shown below, °F;
$|\Delta T_1|$ = absolute value of the range of the temperature difference between the temperature of the outside surface T_o and the temperature of the inside surface T_i of the piping product, assuming moment generating equivalent linear temperature distribution, °F.

This equation calculates the peak stress-intensity range in the pipe, and the alternating stress intensity is one-half the peak stress-intensity range. The fatigue data (alternating stress intensity vs number of cycles to failure) are given in Tables I-9.1 and I-9.2.2. of the Code.[28]

To use Eqs. (1) and (2) [Code Eqs. (10) and (11)], the outside circumferential membrane stress, outside axial bending stress, the thermal stresses from the linear temperature gradient through the wall, and the nonlinear temperature gradient through the wall were needed. In our particular problem, no thermal stress caused by structural discontinuity or material discontinuity was considered. For comparison with the crack-growth studies, the thermal stresses used in the fatigue studies were calculated using the reanalyzed thermal transients.[26] Each transient was digitized, and the following equations were numerically integrated by using an adaptive quadrature routine based on the Newton-Cotes Formulas.[29]

$$T_{AVG} = \frac{1}{t} \int_{-\frac{t}{2}}^{\frac{t}{2}} T(y)dy \ , \tag{3}$$

$$\Delta T_1 = \frac{12}{t^2} \int_{-\frac{t}{2}}^{\frac{t}{2}} y \ T(y)dy \ , \tag{4}$$

$$\Delta T_2 = \max\left(|T_0 - T_{AVG}| - \frac{1}{2}|\Delta T_1|, |T_i - T_{AVG}| - \frac{1}{2}|\Delta T_1|, 0\right) . \tag{5}$$

The newly calculated thermal stresses plus the other needed stress results were taken from Table 6 and are listed in Table 7.

A computer code was written that automatically follows the procedures given in Figs. I-9.2.1 and I-9.2.2 of Ref. 28 and uses Eqs. (1) and (2) to calculate the primary plus secondary stress range and the peak stress intensity and, in turn, uses these equations to calculate the fatigue damage for each cycle given in Table 7.

Six different fatigue analyses were performed using Sect. III[27] procedures. In the first, it was assumed that the area of interest was away

Table 7. Tabulated stress used in Eqs. (1) and (2)

[Code Eqs. (10) and (11)]

Transient	$\frac{P_o D_o}{2t}$	$\frac{D_o}{2I} M$	ΔT_1	$\frac{E\alpha}{2(1-\nu)} \Delta T_1$	ΔT_2	$\frac{E\alpha}{1-\nu} \Delta T_2$
a, b	15,200	6,700	18	3,268	1	411
c, d	750	560	17	3,095	3	952
e, f	1,500	280	7	1,273	2	567
g	3,450	1,250	48	8,772	30	11,095
l	3,740	1,680	75	13,802	51	18,573
m	15,200	4,200	193	35,434	91	33,364
h	21,250	4,610	18	3,268	1	411
OBE	15,260					
SSE	15,500					
Normal plant variations	340			1,090		
Vib.	1,000	1,000				

from the weld and no fatigue strength reduction factors were used. In the second it was assumed that the area was a flush weld; in the third analysis, it was assumed that the area was in an as-welded condition; in the fourth analysis, the maximum fatigue strength reduction factor as specified in the Code[30] was applied to the peak stresses; and in the fifth analysis, the stress concentration effect of the flaw that is assumed to exist was taken into consideration. The fatigue reduction factor for a short crack 0.05 in. deep is 2.5 according to Langer.[31] The sixth analysis was based on a combination of the second analysis (flush weld) and the fifth analysis (stress concentration factor for a crack), which was developed by multiplying these two stress indices together. The stress indices used for these six analyses are given in Table 8. The results of the fatigue analyses are given in Tables 9–14. The fatigue analyses gave very low usage factors, and the number of lifetimes required to produce a usage factor of 1.0 for each case is given in Table 15. As can be seen, the calculated lifetimes for the fatigue analyses vary from 13,000 for the straight pipe to 14 for the highest possible stress concentration case.

Table 8. Stress indices used in fatigue stress calculations

Case	Description	Internal pressure		Moment loading		Thermal loading	
		C_1	K_1	C_2	K_2	C_3	K_3
1	Straight pipe	1.0	1.0	1.0	1.0	1.0	1.0
2	Flush weld	1.0	1.1	1.0	1.1	0.6	1.1
3	As-welded	1.0	1.2	1.0	1.8	0.6	1.7
4	Highest possible stress concentration	1.0	5.0	1.0	5.0	1.0	5.0
5	Stress concentration for crack	1.0	2.5	1.0	2.5	1.0	2.5
6	Stress concentration for crack and flush weld	1.0	2.75	1.0	2.75	0.6	2.75

Table 9. Section III fatigue analysis results for straight pipe with fatigue strength reduction factors all equal to 1.0

Event	n_i	S_a (ksi)	N_i	$U_i = n_i/N_i$
Startup/shutdown	500	12.8	$>10^{11}$	0
Plant loading/plant unloading	15,000	2.7	$>10^{11}$	0
Step increase/step decrease	2,000	1.8	$>10^{11}$	0
Reactor trip and recover at startup	400	12.3	$>10^{11}$	0
Loss of flow and abnormal loss of load	80	18.9	$>10^{11}$	0
Loss of secondary pressure	5	44.1	65,166	0.000077
Hydrotest to 3125 psig, 400°F	10	14.8	$>10^{11}$	0
Operating basis earthquake	200	7.6	$>10^{11}$	0
Safe shutdown earthquake	1	7.8	$>10^{11}$	0
Vibrations	2.1×10^{10}	1.0	$>10^{11}$	0
Normal plant variations	2.1×10^{6}	0.7	$>10^{11}$	0
$U = \Sigma U_i$				0.000077

Table 10. Section III fatigue analysis results for flush weld ($K_1 = K_2 = K_3 = 1.1$)

Event	n_i	S_a (ksi)	N_i	$U_i = n_i/N_i$
Startup/shutdown	500	14.0	$>10^{11}$	0
Plant loading/plant unloading	15,000	2.9	$>10^{11}$	0
Step increase/step decrease	2,000	2.0	$>10^{11}$	0
Reactor trip and recover at startup	400	13.0	$>10^{11}$	0
Loss of flow and abnormal loss of load	80	19.9	4,861,600	0.000017
Loss of secondary pressure	5	46.8	47,013	0.000106
Hydrotest to 3125 psig, 400°F	10	16.2	$>10^{11}$	0
Operating basis earthquake	200	8.4	$>10^{11}$	0
Safe shutdown earthquake	1	8.5	$>10^{11}$	0
Vibrations	2.1×10^{10}	1.1	$>10^{11}$	0
Normal plant variations	2.1×10^{6}	0.8	$>10^{11}$	0
$U = \Sigma U_i$				0.000123

Table 11. Section III fatigue analysis results for as-welded condition ($K_1 = 1.2$, $K_2 = 1.8$, $K_3 = 1.7$)

Event	n_i	S_a (ksi)	N_i	$U_i = n_i/N_i$
Startup/shutdown	500	18.1	12,337,000	0.000041
Plant loading/plant unloading	15,000	4.1	$>10^{11}$	0
Step increase/step decrease	2,000	2.5	$>10^{11}$	0
Reactor trip and recover at startup	400	16.2	$>10^{11}$	0
Loss of flow and abnormal loss of load	80	24.8	1,474,000	0.000054
Loss of secondary pressure	5	59.7	13,903	0.000360
Hydrotest to 3125 psig, 400°F	10	19.9	4,807,500	0.000002
Operating basis earthquake	200	13.7	$>10^{11}$	0
Safe shutdown earthquake	1	14.0	$>10^{11}$	0
Vibrations	2.1×10^{10}	1.5	$>10^{11}$	0
Normal plant variations	2.1×10^{6}	1.1	$>10^{11}$	0
$U = \Sigma U_i$				0.000457

Table 12. Section III fatigue analysis results using highest possible stress concentration

($K_1 = K_2 = K_3 = 5.0$)

Event	n_i	S_a (ksi)	N_i	$U_i = n_i/N_i$
Startup/shutdown	500	63.1	10,647	0.046960
Plant loading/plant unloading	15,000	11.5	$>10^{11}$	0
Step increase/step decrease	2,000	7.9	$>10^{11}$	0
Reactor trip and recover at startup	400	39.2	123,510	0.003239
Loss of flow and abnormal loss of load	80	57.3	16,987	0.004709
Loss of secondary pressure	5	153.8	444	0.011262
Hydrotest to 3125 psig, 400°F	10	73.0	5,824	0.001717
Operating basis earthquake	200	38.2	143,330	0.001395
Safe shutdown earthquake	1	38.8	131,185	0.000008
Vibrations	2.1×10^{10}	5.0	$>10^{11}$	0
Normal plant variations	2.1×10^{6}	3.6	$>10^{11}$	0
$U = \Sigma U_i$				0.069290

Table 13. Section III fatigue analysis results using stress concentration factor for crack

($K_1 = K_2 = K_3 = 2.5$)

Event	n_i	S_a (ksi)	N_i	$U_i = n_i/N_i$
Startup/shutdown	500	31.7	433,020	0.001155
Plant loading/plant unloading	15,000	6.0	$>10^{11}$	0
Step increase/step decrease	2,000	4.1	$>10^{11}$	0
Reactor trip and recover at startup	400	22.4	2,170,600	0.000184
Loss of flow and abnormal loss of load	80	33.3	311,970	0.000256
Loss of secondary pressure	5	85.2	3,229	0.001548
Hydrotest to 3125 psig, 400°F	10	36.6	179,120	0.000056
Operating basis earthquake	200	19.1	7,326,800	0.000027
Safe shutdown earthquake	1	19.4	6,219,700	0
Vibrations	2.1×10^{10}	2.5	$>10^{11}$	0
Normal plant variations	2.1×10^{6}	1.8	$>10^{11}$	0
$U = \Sigma U_i$				0.003226

Table 14. Section III fatigue analysis results using stress concentration for crack[a] and flush weld in combination

($K_1 = K_2 = K_3 = 2.75$)

Event	n_i	S_a (ksi)	N_i	$U_i = n_i/N_i$
Startup/shutdown	500	34.8	238,910	0.002093
Plant loading/plant unloading	15,000	6.5	$>10^{11}$	0
Step increase/step decrease	2,000	4.5	$>10^{11}$	0
Reactor trip and recover at startup	400	24.0	1,622,000	0.000247
Loss of flow and abnormal loss of load		35.7	205,890	0.000389
Loss of secondary pressure			2,417	0.002069
Hydrotest to 3125 psig, 400°F	10		107,510	0.000093
Operating basis earthquake	200		3,126,200	0.000064
Safe shutdown earthquake	1		2,826,700	0
Vibrations	2.1		$>10^{11}$	0
Normal plant variations	2.1		$>10^{11}$	0
$U = \Sigma U_i$				0.004955

[a]A 0.050-in.-deep by 3/16-in.-long semielliptical surface crack.

Table 15. Number of lifetimes required to produce usage factor of 1.0

Case	Number of lifetimes
Straight pipe	13,000
Flush weld	8,100
As-welded	2,200
Highest SCF	14
Crack[a] SCF	310
Crack[a] SCF and flush weld	201

[a]A 0.050-in.-deep by 3/16-in.-long semielliptical surface crack.

4. FATIGUE CRACK-GROWTH ANALYSIS

Section XI of the *ASME Boiler and Pressure Vessel Code*[3] provides acceptance standards for defects found during inservice inspections. For no defects or defects with a size less than the specified acceptance levels, the Code does not require any remedial action; the component is considered acceptable. For defect sizes larger than the acceptance levels, an evaluation using fracture mechanics (taking into account the factors discussed in nonmandatory Appendix A of Sect. XI) can be performed to show whether crack growth will cause failure before the next inspection or end-of-life. If this analysis is successful, the component is conditionally acceptable, and no repair or replacement is required. However, an upgraded inspection plan is specified to monitor any future crack growth.

The criteria in Sect. XI for acceptance of flaw indications without evaluation (for ferritic steels with nominal yield strength below 50,000 psi) were based on provisions for protection against nonductile failure contained in Appendix G of Sect. III of the Code.[22] These provisions provided the basis for using a reference flaw of depth equal to 1/4 the wall thickness t and length ℓ equal to 1-1/2 times the thickness. As a measure of conservatism to establish an allowable acceptance limit for a surface flaw, the flaw depth a of 1/10 of that postulated in Appendix G of Sect. III was selected (i.e., $a_{XI} = a_{III}/10$). Fracture mechanics stress-intensity factor solutions from Appendix G were then applied to determine equivalent surface and subsurface flaw size acceptance limits for different flaw geometries. Figures 2 and 3 (taken from Ref. 32) illustrate the approach and results for surface (Fig. 2) and subsurface (Fig. 3) flaws. Subsurface flaw sizes can be larger, as shown in Fig. 3, due to lower stress-intensity factor values for equivalent size flaws.

For austenitic steel piping, application of LEFM is not suitable for fracture analysis due to the fully plastic conditions that are often developed for this highly ductile material prior to fracture. As a conservative basis for the development of acceptance standards for austenitic steels, a net-section ductile yielding criterion was initially used taking advantage of the high strain hardening of austenitic steels. Although the permissible flaw sizes derived (using the net-section yielding approach) are conservative for strain hardening materials, the standards for acceptance of flaw indications without evaluation were even more conservatively lowered to correspond to the range of flaw sizes detectable by presently used ultrasonic techniques. Figure 4 illustrates this difference between the permissible flaw sizes from the net-section yield approach and the range of allowable indications based on flaw detectability threshold. For consistency with the ferritic steel acceptance standards, a flaw with an aspect ratio a/ℓ of 1/6 was taken as the normalizing point in defining the ultrasonic detectability threshold.

The inservice extension of flaws may be estimated by a fatigue crack-growth analysis. Development of this analysis is dependent on knowledge of the flaw size, applied stresses, and an appropriate stress-intensity factor solution. Two analytical procedures for calculating the stress intensity factor are the *ASME Boiler and Pressure Vessel Code* Sect. XI

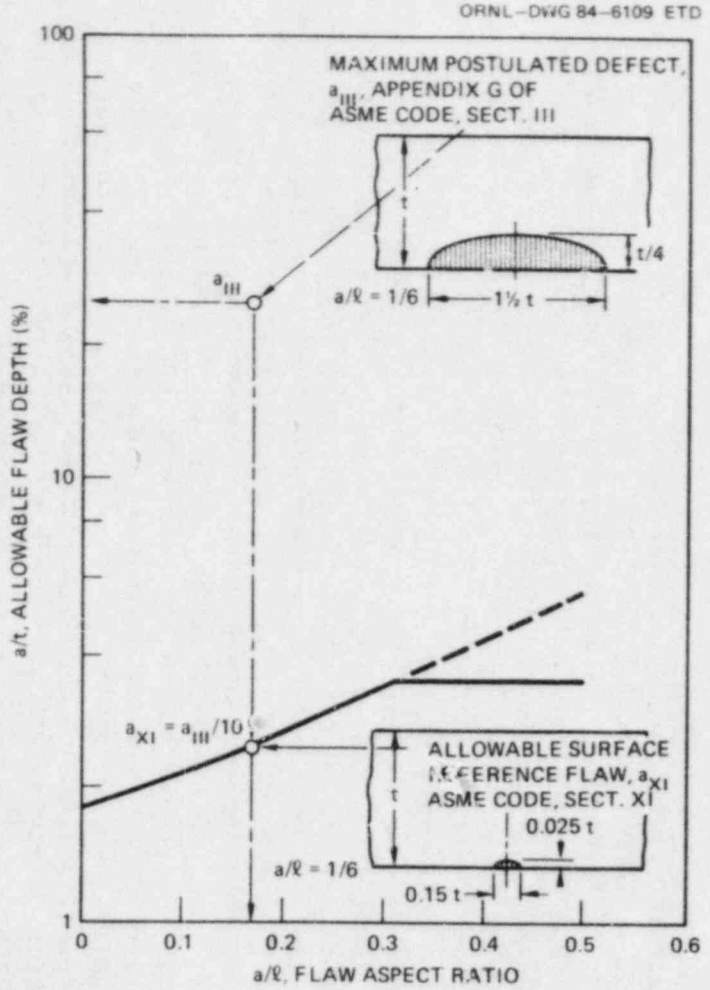

Fig. 2. Relationship between maximum postulated defect and allowable surface indications (from Ref. 22).

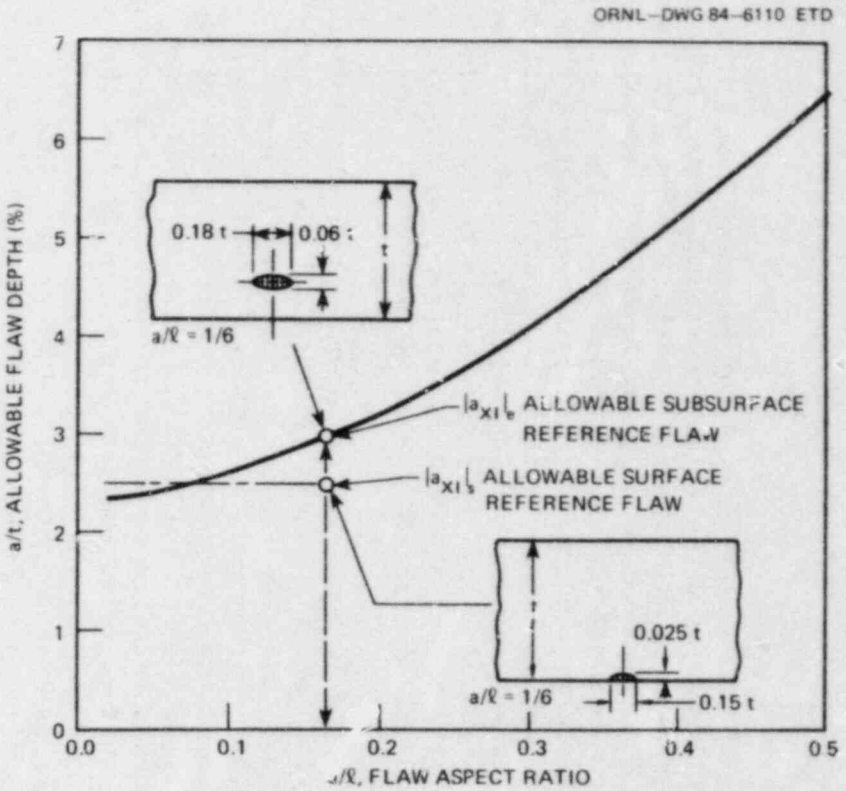

Fig. 3. Relationship between surface and subsurface reference flaws (from Ref. 32).

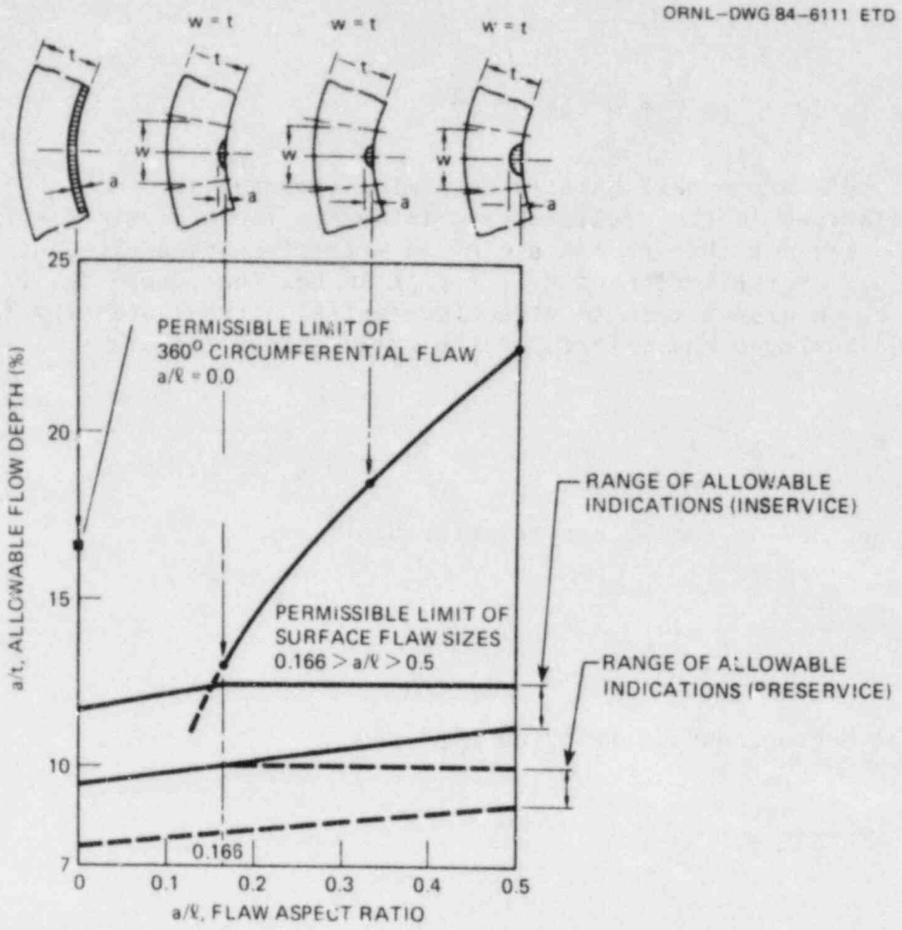

Fig. 4. Permissible surface flaw size limits and allowable indication standards vs flaw aspect ratio (from Ref. 32).

Appendix A approach and a more refined solution based on influence function techniques.[33] The following discussion summarizes fatigue crack-growth behavior and the estimated crack-growth response based on the two stress-intensity factor solutions.

4.1 Fatigue Crack-Growth Behavior

Fatigue crack propagation behavior can generally be described by a power law in the Paris or stage II region of crack propagation. This power law relates the incremental fatigue crack-growth rate da/dN to the stress-intensity factor range ΔK in the following manner:

$$da/dN = C\ (\Delta K)^m\ , \qquad (6a)$$

or

$$\log da/dN = \log C + m \log \Delta K \ , \tag{6b}$$

where C and m are experimentally determined constants.

Variations in the cyclic stress-intensity factor ratio $R = K_{min}/K_{max}$ are accounted for through the use of an effective stress-intensity factor value K_{eff}. Substitution of K_{eff} for ΔK in Eq. (6a) gives Eq. (7), which relates crack-growth rate to effective applied stress-intensity factor range and includes the effects of the cycle stress ratio:

$$\frac{da}{dN} = C\,(K_{eff})^m \ . \tag{7}$$

K_{eff} is defined in the Walker relationship[34] as

$$K_{eff} = \frac{\Delta K}{(1 - R)^n} \ , \tag{8}$$

or in the Rabbé-Lieurade relationship[35] as

$$K_{eff} = \frac{\Delta K}{(1 - R/\alpha)} \ , \tag{9}$$

where α and n are material-dependent parameters. Other variables such as environment, cyclic frequency, stress-intensity threshold, residual stresses, and crack retardation may affect the fatigue crack propagation behavior depending on the material and existing conditions.

4.2 Section XI Analysis

For a Sect. XI Appendix A analysis, a stress-intensity factor K_I is defined as:

$$K_I = \sigma_m M_m \sqrt{\pi} \sqrt{a/Q} + \sigma_b M_b \sqrt{\pi} \sqrt{a/Q} \ , \tag{10}$$

where

σ_m, σ_b = membrane and bending stresses, respectively;
M_m, M_b = membrane and bending free surface correction factors[32] for a flat plate, respectively;
a = flaw depth for a surface flaw,
Q = flaw shape parameter.

Membrane and bending stresses are determined from the linearization of the actual through-wall axial stress profile as specified in Sect. XI Appendix A of the Code. The linearization technique defines two stresses (at the outside surface and depth of a surface flaw) and uses these positions in determining an equivalent linear representation of stress distribution. Parameters Q, M_m, and M_b are determined from Appendix A curves that are considered to be conservative.[32] A stress-intensity range is defined as

$$\Delta K = [\Delta\sigma_m M_m + \Delta\sigma_b M_b]\sqrt{\pi}\sqrt{a/Q} . \qquad (11)$$

This range is substituted into the fatigue crack-growth law and integrated to give a change in flaw size Δa for a corresponding number of fatigue cycles ΔN.

4.3 Computer Code Analysis

The Electric Power Research Institute (EPRI) computer code DRIVE was developed to calculate stress-intensity factors for surface cracks in pipes by use of influence functions.[33] Modifications in the computer code to incorporate fatigue crack-growth laws allow a more accurate calculation of the crack-growth response than the Sect. XI approach, because the conservatism of the free surface corrections for plates is eliminated. The free surface correction factors adjust the basic values of the stress-intensity factors to account for finite thickness and flaw location effects.

4.4 Material Considerations

The effect of various parameters on the fatigue crack propagation behavior of a 316 stainless steel weld defect needs to be considered to complete a fatigue crack-growth analysis. Applicable fatigue crack-growth data and parameters such as environment, frequency, stress-intensity factor threshold, residual stresses, and crack retardation were investigated.

4.4.1 Crack-growth data

The fatigue crack-growth analysis of a 316 stainless steel weld defect requires compilation of fatigue crack-growth data in a PWR environment. A data base of crack-growth results for 316 stainless steel product forms in air and PWR environments was compiled with assistance from the Battelle/EPRI data base management system, EDEAC.[36] Fatigue crack propagation rates for 316 stainless steels differ from those of other austenitic stainless steels under similar conditions;[37] therefore, only 316 stainless steel plate, casting, and weldment data were utilized. Figure 5

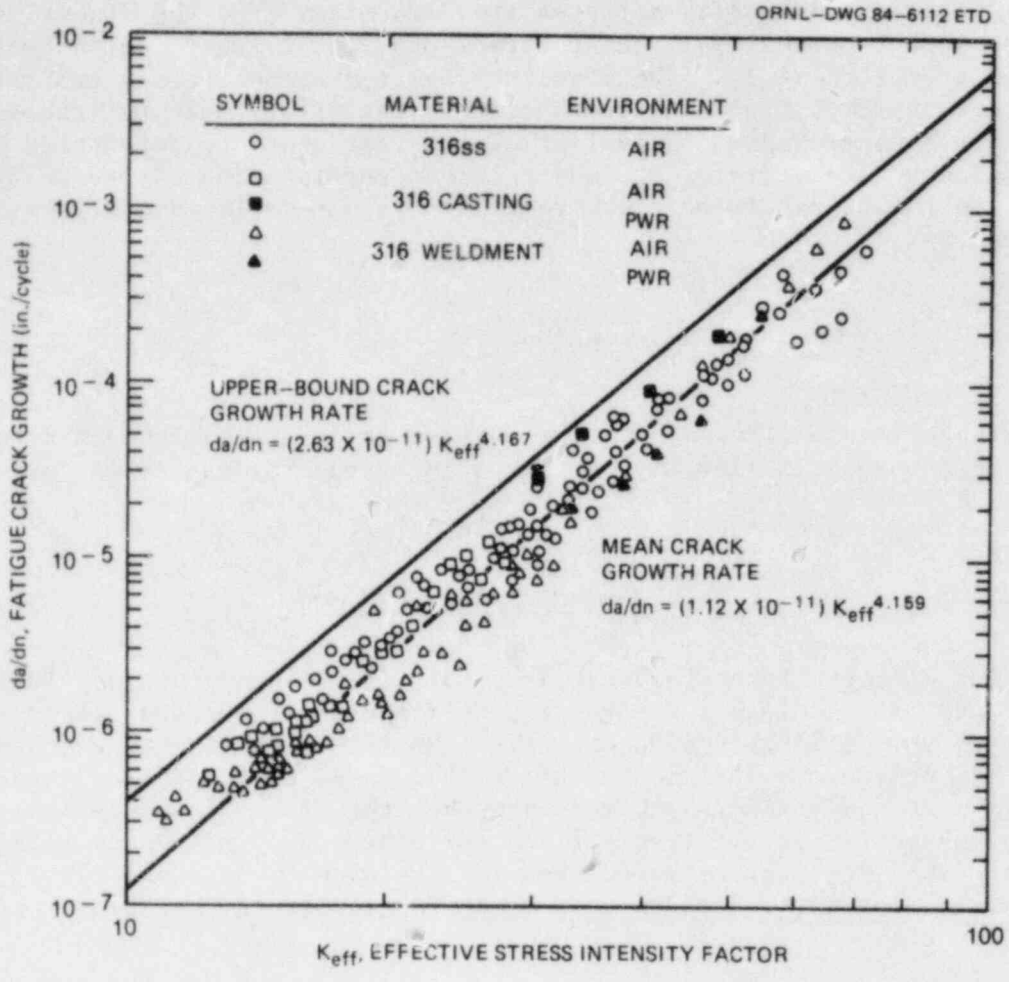

Fig. 5. Compiled fatigue crack-growth data for 316 stainless steel.

shows weldment, casting, and plate data separated by material form.[38-40] Growth rates in austenitic stainless steel weldments are generally equivalent to or lower than growth rates in wrought stainless steels; therefore, all 316 stainless steel product forms were included in the analyzed data base.[41] A statistical regression was performed to determine the parameters C and m of Eq. (6a). Figure 5 also shows a graphical upper bound to the data and its corresponding C and m parameters.

The fatigue crack-growth rate data are plotted as a function of K_{eff} in Fig. 5. As described in Sect. 4.1, K_{eff} is a function of the stress-intensity factor ΔK and the cyclic stress ratio R. Whether defined as in Eq. 8 (Walker) or Eq. 9 (Rabbé-Lieurade), negligible differences occur between the two methods of calculating K_{eff} for small R ratios ($0 \leq R \leq 0.2$). The R ratios of the compiled 316 stainless steel data were to ≤ 0.2; thus, one plot (Fig. 5) of da/dN vs K_{eff} was utilized for the data, where K_{eff} was in the form of a Walker relationship.

4.4.2 Other fatigue crack propagation parameters

A variety of parameters affect the fatigue crack propagation rates of austenitic stainless steels. These parameters include environment, frequency, stress intensity threshold, residual stresses, and crack retardation.

Temperature and environment can have a profound effect on fatigue crack growth. As mentioned previously, both air and PWR environments were included in the data base. Reference 41 indicated a negligible difference between air and PWR environment. The temperature range chosen was 500 to 800°F, which encompasses the reactor operating temperature of 550°F and is conservative. The effect of frequency has been assumed to be negligible at these temperatures.[41]

A large number of cycles at very low stresses can result in crack growth to a critical flaw size within the design life of the reactor if there is no stress-intensity factor threshold. For this reason, calculations both included and excluded a stress-intensity factor threshold as shown in Tables 16–21 (Sect. 4.7). A threshold value for 316 stainless steel welds in a PWR environment has not yet been determined, but there are published values for stainless steels in air environments.[9,10,42] Threshold values of 4.6 ksi$\cdot\sqrt{\text{in.}}$ and 2.6 ksi$\cdot\sqrt{\text{in.}}$ were utilized in the calculations.

Residual stresses were ignored in this study. There are currently no generally accepted means for taking crack retardation into account. Crack retardation occurs when a high cyclic stress blunts the crack tip and causes less crack growth to occur until the crack grows out of the blunted crack stress field. Ignoring crack retardation will be conservative, and this approach was taken in the analyses.

4.5 Thermal and Stress Analyses

In a crack-growth analysis, a stress-intensity factor range ΔK must be calculated as indicated in Sect. 4.2. This calculation is dependent on an existing time-dependent axial stress distribution for each of the transients presented earlier. This time dependence is primarily due to the thermal stress component of the total axial stress distribution.

A thermal analysis was first performed to determine the temperature gradients for the hot-leg pipe location of concern for all transients considered.[26] Most of the input data for the Zion-1 hot-leg came from Refs. 6 and 9; in some cases, the graphical fluid temperature data in Ref. 9 did not agree with tabulated data in Ref. 6, probably because of typographical errors.

The radial temperature gradient results were then analyzed to allow calculation of axial thermal stress distributions through the pipe wall assuming no end restraint.[43] One-dimensional temperature distributions for various times in each transient were generated; with the maximum dead weight, thermal expansion, and pressure stresses determined in Ref. 6, the total axial stress distributions as a function of time were determined. Figure 6 shows an example of the total stress gradients at different times for Transient e, f (Table 1). An LEFM approach was applied

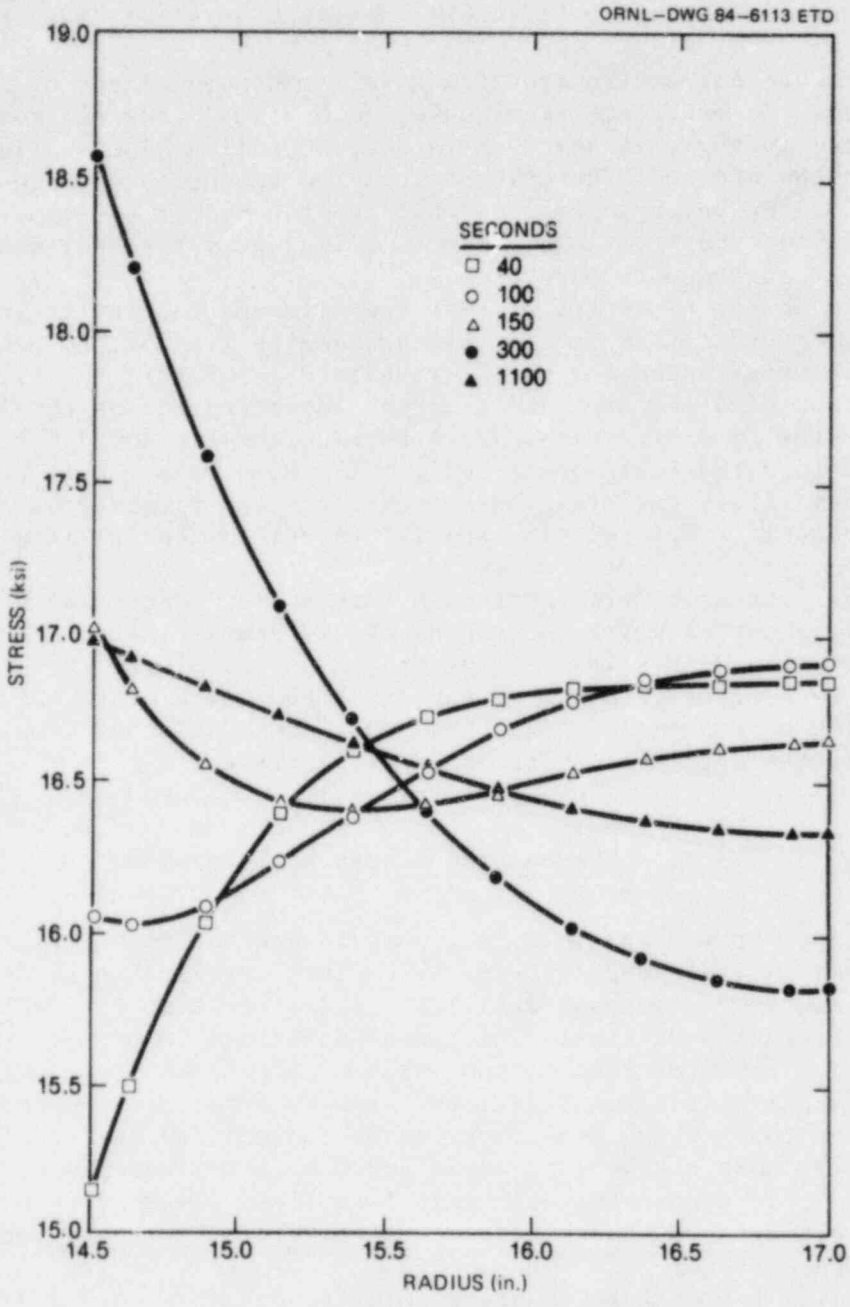

Fig. 6. Axial stress distribution through the pipe wall as function of time for step increase/decrease, Transients e, f (from Ref. 43).

to all transients, including Transient m where the maximum stress at the inside surface exceeded yield.

4.6 Critical Flaw Size

To determine if fatigue would cause failure of the flawed section, a failure criterion based on limit load was applied. The criterion was based on the new Appendix C to the ASME Code.[44] A critical flaw depth to thickness ratio a/t is determined as a function of flaw length to pipe circumference and applied stress conditions. Thus, as the flaw grows in length, the critical a/t can change. The margin of safety for unflawed piping is maintained in this approach for the section of the pipe reduced by the flaw area (net section area); the critical crack depth is also never allowed to exceed 75% of the wall thickness.

4.7 Results of Crack-Growth Analyses

Two approaches were taken to calculate the crack growth response of the hot-leg safe-end weld defect. The first approach closely follows the guidelines of Appendix A Sect. XI of the *ASME Boiler and Pressure Vessel Code*, while the second approach utilizes more current methodologies and mean material properties.

4.7.1 Section XI analyses

For the most severe stress distribution as a function of time for each transient, the actual stress distribution is approximated using the linearization technique illustrated in Appendix A Sect. XI of the Code. Membrane and bending stresses are determined from the linearized stress distribution, and stress ranges $\Delta\sigma_m$ and $\Delta\sigma_b$ are determined based on the assumption that the transients occur during steady state operation (with the exception of the hydrostatic test). Parameters M_m, M_b, and Q along with $\Delta\sigma_m$ and $\Delta\sigma_b$ are functions of the crack depth and are calculated for each cycle to determine an updated ΔK. This ΔK range is substituted into the Rabbé-Lieurade relationship or Walker relationship, along with the conservative upper-bound crack growth constants C and m, and integrated for an increase in flaw size for a given number of cycles ΔN. The spectrum of loading is the same as that for the Sect. III fatigue analysis.

Two approaches based on the calculated values of M_m and M_b were used in the Sect. XI Appendix A analyses. The first assumed a constant aspect ratio (a/2c), while the second allowed the aspect ratio to vary. M_b is defined for the depth dimension ($\beta = 0°$) and length dimension ($\beta = 90°$), while M_m is only defined in the depth dimension. Thus, assuming a constant aspect ratio eliminates the need for a correction factor in the length dimension. Assigning M_m a value of one in the length dimension allows separate calculations of flaw growth in the depth and length dimensions.

The calculated crack-growth responses of the two hot-leg safe-end weld defects are shown in Tables 16–19. Analyses were conducted for the

Table 16. Section XI analyses of Sect. III allowable flaw (a = 0.050 in.) for 40-year design lifetime

	Stress-intensity factor threshold (ksi·√in.)	Final[a] flaw depth (in.)	Final[b] flaw length (in.)	Final[c] aspect ratio
Constant aspect ratio				
Walker relationship	4.6	0.0502	0.1882	0.267
	2.6	0.0502	0.1882	0.267
Rabbé-Lieurade relationship	4.6	0.0502	0.1882	0.267
	2.6	0.0502	0.1882	0.267
	None	0.0733	0.2750	0.267
Variable aspect ratio				
Walker relationship	4.6	0.0502	0.1901	0.264
	2.6	0.0502	0.1901	0.264
Rabbé-Lieurade relationship	4.6	0.0502	0.1901	0.265
	2.6	0.0502	0.1895	0.265
	None	0.600	33.106	0.018[d]

[a]Initial flaw depth 0.050 in.

[b]Initial flaw length 0.1875 in.

[c]Initial aspect ratio 0.267.

[d]Flaw reached critical size prior to end of 40-year design lifetime.

Table 17. Number of 40-year lifetimes until critical flaw size for Sect. III allowable flaw (a = 0.050 in.) (Sect. XI analysis)

	Stress-intensity factor threshold (ksi·√in.)	Number of 40-year lifetimes	Critical[a] flaw depth (in.)	Critical[b] flaw length (in.)	Critical[c] aspect ratio
Constant aspect ratio					
Walker relationship	4.6	316	1.875	7.03	0.267
Rabbé-Lieurade relationship	4.6	331	1.875	7.03	0.267
	2.6	328	1.883	7.06	0.267
	None	2	1.875	7.03	0.267
Variable aspect ratio					
Walker relationship	4.6	155	1.229	17.0	0.072
Rabbé-Lieurade relationship	4.6	181	1.521	14.21	0.107
	2.6	173	0.511	39.62	0.013
	None	0.85	0.600	33.11	0.018

[a]Initial flaw depth 0.050 in.

[b]Initial flaw length 0.1875 in.

[c]Initial aspect ratio 0.267 in.

Table 18. Section XI analyses for Sect. XI allowable preservice flaw (a = 0.216 in.) for 40-year design lifetime

	Stress-intensity factor threshold (ksi·√in.)	Final[a] flaw depth (in.)	Final[b] flaw length (in.)	Final[c] aspect ratio
Constant aspect ratio				
Walker relationship	4.6	0.218	0.758	0.288
	2.6	0.218	0.759	0.288
Rabbé-Lieurade relationship	4.6	0.218	0.758	0.288
	2.6	0.218	0.758	0.288
	None	1.877	6.517	0.288
Variable aspect ratio				
Walker relationship	4.6	0.218	0.800	0.273
	2.6	0.218	0.810	0.269
Rabbé-Lieurade relationship	4.6	0.218	0.788	0.277
	2.6	0.213	0.788	0.276
	None	0.726	25.73	0.028[d]

[a]Initial flaw depth 0.216 in.

[b]Initial flaw length 0.75 in.

[c]Initial aspect ratio 0.288.

[d]Flaw reached critical size prior to end of 40-year design lifetime.

Table 19. Number of 40-year lifetimes until critical flaw size for Sect. XI allowable preservice flaw (a = 0.216 in.) (Sect. XI analyses)

	Stress-intensity factor threshold (ksi·√in.)	Number of 40-year lifetimes	Critical[a] flaw depth (in.)	Critical[b] flaw length (in.)	Critical[c] aspect ratio
Constant aspect ratio					
Walker relationship	4.6	104	1.875	6.511	0.288
Rabbé-Lieurade relationship	4.6	109	1.875	6.512	0.288
	None	0.55	1.877	6.517	0.288
Variable aspect ratio					
Walker relationship	4.6	33	1.238	16.90	0.073
Rabbé-Lieurade relationship	4.6	40	1.549	14.171	0.109
	None	0.12	0.726	25.73	0.028

[a]Initial flaw depth 0.216 in.

[b]Initial flaw length 0.75 in.

[c]Initial aspect ratio 0.288 in.

surface flaw model decided on by the DET (a = 0.050 in.), for a larger preservice internal (subsurface) indication treated as a surface flaw (a = 0.216 in.), and for a still larger internal (subsurface) indication treated as a surface flaw (a = 0.2745 in.). Results for the inservice flaw are not given in the tables. Results for all three cracks are shown in Fig. 7. Identification of the type of relationship (Rabbé-Lieurade or Walker) and the stress-intensity threshold are given for each calculation along with the final flaw depth, length, and aspect ratio.

In Tables 16 and 18, the Sect. XI results are given for calculations of the final flaw size after one 40-year design lifetime. For the DET suggested flaw, negligible crack growth occurred for all calculations except for those that excluded a stress-intensity factor threshold. When the aspect ratio was allowed to vary and the stress-intensity factor threshold was excluded, the smaller flaw reached a critical flaw size prior to the end of the 40-year design lifetime. For the larger preservice flaw model (a = 0.216 in.), a similar result was obtained in which negligible crack growth occurred for all calculations except those that excluded a stress-intensity factor threshold.

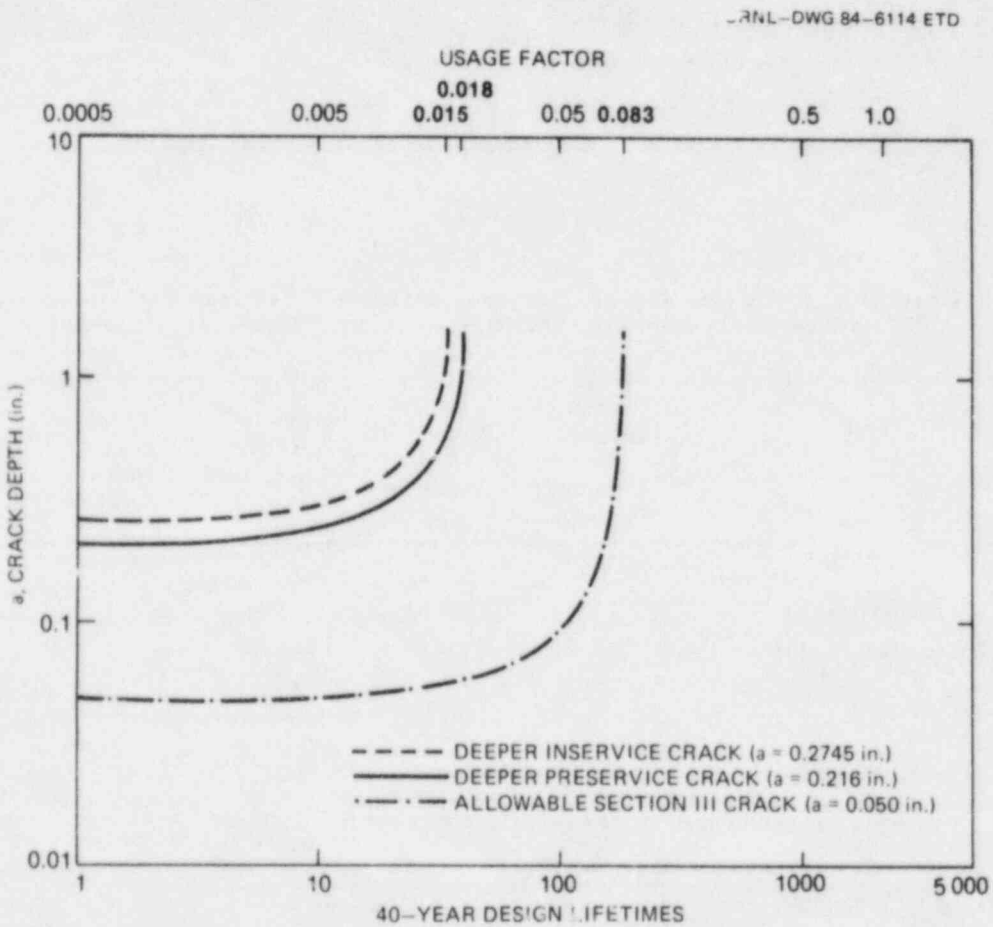

Fig. 7. Crack depth determined using Sect. XI analysis as function of 40-year design lifetimes and usage factor.

Crack-growth response as a function of 40-year design lifetimes was calculated for the two flaw models discussed previously. The number of 40-year design lifetimes until a critical flaw size is reached is shown in Tables 17 and 19. Additional calculations using a Rabbé-Lieurade relationship and a 4.6-ksi$\sqrt{\text{in.}}$ stress-intensity factor threshold were made for a Sect. XI allowable inservice indication (a = 0.2745 in.). Thirty-four design lifetimes were needed before a critical flaw depth of 1.54 in. was obtained for the inservice indication.

In the Sect. III fatigue analyses, 2188 lifetimes were required to give a usage factor of one for the as-welded condition. Assuming a usage factor of one denotes failure,* a "critical usage factor," which is the ratio of the calculated number of lifetimes to 2188, can be assigned to each of the flaw sizes. Figure 7 shows crack growth determined using the Rabbé-Lieurade relationship and a variable aspect ratio in a Sect. XI analysis as a function of both 40-year design lifetimes and usage factor. Critical usage factors of 0.015, 0.018, and 0.083 correspond to the deeper inservice flaw (a = 0.2745 in.), deeper preservice flaw (a = 0.216 in.), and the shallow flaw (a = 0.050 in.), respectively. Note that there is only a small difference between the results for the preservice and inservice flaws. Therefore, tabular results were not given for the inservice crack. Both gave total lifetimes that were a fraction of the Sect. III fatigue life for this component in the as-welded condition.

4.7.2 Computer code analyses

Crack-growth response was also calculated using the EPRI computer code DRIVE.[33] This more refined analysis calculated stress-intensity factors for surface cracks in pipes using influence functions and the exact stress distribution for the highest ΔK anytime in the transients. Crack-growth rate constants C and m from the regression analyses were used for one set of calculations, and another set of calculations utilized the upper-bound constants for direct comparison with the Sect. XI analyses. Calculations of the final flaw size for a 40-year design lifetime were determined using both the Walker and Rabbé-Lieurade relationships. The crack-growth response after a 40-year design lifetime was calculated for the two flaw sizes as shown in Tables 20 and 21. The mean fatigue crack-growth analyses showed very little flaw growth as compared with the analyese using an upper-bound crack-growth law. Comparisons made between the Sect. XI analyses and the DRIVE computer code analyses for similar conditions showed negligible difference and very little crack growth, although the Sec. XI analyses consistently showed greater growth in the length dimensions as compared with the computer code analyses.

---

*In reality, failure would not be expected to occur until the usage factor exceeded one by some undefined margin. The Code fatigue design curves used in determining the usage factor were derived from fatigue test data from smooth specimens reduced by a factor of 20 on cycles or 2 on stress, whichever is greater. However, a summary of many tests on prototypic vessels[16] shows that the design fatigue curves are very realistic; that is, the actual design margin is usually much less than 20 on cycles.

Table 20. Computer code DRIVE analysis for Sect. III allowable flaw (a = 0.050 in.) for a 40-year design lifetime

	Stress-intensity factor threshold (ksi·√in.)	Final[a] flaw depth (in.)	Final[b] flaw length (in.)	Final[c] aspect ratio
Upper-bound growth rate				
Walker relationship	4.6	0.0503	0.1878	0.268
Rabbé-Lieurade relationship	4.6	0.0502	0.1878	0.267
	None	0.1316	0.3168	0.415
Mean growth rate				
Walker relationship	4.6	0.0500	0.1875	0.267
Rabbé-Lieurade relationship	4.6	0.0500	0.1875	0.267
	None	0.0517	0.1895	0.273

[a]Initial flaw depth 0.050 in.

[b]Initial flaw length 0.1875 in.

[c]Initial aspect ratio 0.267.

Table 21. Crack computer code DRIVE analyses for Sect. XI allowable preservice flaw (a = 0.216 in.) for a 40-year design lifetime

	Stress-intensity factor threshold (ksi·√in.)	Final[a] flaw depth (in.)	Final[b] flaw length (in.)	Final[c] aspect ratio
Upper bound growth rate				
Walker relationship	4.6	0.219	0.755	0.290
Rabbé-Lieurade relationship	4.6	0.218	0.754	0.289
	None	1.941	3.991	0.486[d]
Mean growth rate				
Walker relationship	4.6	0.216	0.750	0.288
Rabbé-Lieurade relationship	4.6	0.216	0.750	0.288
	None	0.255	0.796	0.320

[a]Initial flaw depth 0.216 in.

[b]Initial flaw length 0.75 in.

[c]Initial aspect ratio 0.288.

[d]Flaw reached critical size prior to end of 40-year design lifetime.

5. DISCUSSION

The Sect. III fatigue analysis for the as-welded condition is the one that would be used by the designer when qualifying this component. The fatigue usage factor was so low that 2200 lifetimes would be required to reach a fatigue usage factor of 1.0. The Sect. XI analysis predicted that a critical flaw size would not be reached until 150 to 330 lifetimes had been expended. Thus, in this case the Sect. III analysis would permit a longer period of operation than a Sect. XI analysis would. Both analyses include design margins, so failure would not be expected even after the allowable period. Relative margins are not known; thus, a clear and direct comparison of the two approaches is not possible. Note that when the stress concentration factor for the assumed flaw was used, the allowable number of lifetimes according to a Sect. III analysis was 310, which is very near the 316 and 321 lifetimes predicted when a Sect. XI analysis was done, assuming a constant aspect ratio for the crack. Furthermore, when the stress concentration factor for the crack was superimposed on the flush weld, the Sect. III analysis gave a prediction of 190 lifetimes, which is very near the predicted lifetimes of 155 and 181 given by the Sect. XI analysis when a variable aspect ratio was allowed.

Generally, the stress levels were at the high-cycle end of the fatigue curve where the factor of 2 on stress was used to generate the design curve from fatigue data. Higher stress levels would have resulted in so much plasticity that LEFM would not have been applicable. Because the crack initiation phase is a relatively high portion of the total life in high-cycle fatigue, the LEFM approach would be expected to be conservative if no cracklike defect happened to be present, since it ignores crack initiation. Even if an initial cracklike defect should exist, some cycling will probably occur before propagation starts.

The earlier study[4] by Anderson, Weidenhamer, and Johns concluded that if a component experiences a high level of cyclic stress that corresponds to a usage factor of 1.0, very small cracks can propagate to sizes that exceed Code-specified limits. That study was the impetus for the current study. The current study is an attempt to answer the principal concerns expressed by the reviewers of Anderson's study. Those concerns were mostly a result of the simplifying assumptions that they used. The specific concerns were

1. the through-the-wall stress distribution was not prototypic;
2. all the loading was assumed to occur at one stress level, which does not account for the variation in loading as demonstrated by operating time histories; and
3. there are very few actual cases in which a component is subjected to stress levels having a usage factor of 1.0.

We will discuss what the current study reveals about each of these concerns.

The first two concerns were addressed by analyzing an actual reactor component for a realistic design loading. Neither appeared to have any real effect, because the fatigue crack growth procedure still predicted a shorter life than the S-N approach.* The effect of the through-the-wall stress distribution on the crack propagation has also been studied by Simonen and Goodrich[45] who found that there was some effect but it was small.

The third concern that there are few actual cases in which a component is subjected to loading conditions that result in a usage factor approaching 1.0 was found to be true for the present generation of pressurized water reactors (PWRs).

For the present study, we decided to limit our research to straight pipe locations. With that limitation, the fatigue usage factor in the primary piping systems of current PWRs is certainly very much less than 1.0. The terminal end of the hot-leg piping was selected because it was the straight pipe location with the highest fatigue usage factor in the primary coolant system of Zion-1. The fatigue usage factor, assuming the weld was left in the as-welded condition, was only 0.0005. It was also the straight pipe location of the highest fatigue usage factor in St. Lucie 2 (Ref. 46). Furthermore, the highest stress intensity occurs at this same location in a German PWR.[47]

However, note the fatigue usage factor at the inside surface of the charging inlet nozzle for St. Lucie 2 was 0.784 according to the design stress report;[46] most (0.700 of the 0.784) came from a reactor trip with loss of flow combined with a loss of charging flow, which resulted in a stress range of 110.08 ksi. Because the primary plus secondary stress range of 83.48 ksi exceeded the $3S_m$ value, it was necessary to apply a plastic stress correction factor K_e to determine the S_{alt} value of 185.43 ksi that was used to enter the S-N fatigue curve to find the allowable number of cycles. Therefore, although the straight pipe analysis of the present report did not approach a usage factor of 1.0 with a constant amplitude stress cycle, there are some cases that do; one example is the inside surface of the St. Lucie 2 charging inlet nozzle. However, note that so much inelastic straining occurs at that location that LEFM would be of questionable validity. Furthermore, it is in this low-cycle fatigue regime that the S-N fatigue curve approach has best been demonstrated to be reliable by tests.

Precise determination of the threshold stress-intensity factor is a difficult experimental task. The use of a threshold stress-intensity factor in our calculations was very important in determining the effects of cycles with low stress ranges. Otherwise, results were obtained that predicted failure at such low lifetimes that they did not appear to be realistic. It made very little difference, however, whether the value was 2.6 ksi$\cdot\sqrt{\text{in.}}$ or 4.6 ksi$\cdot\sqrt{\text{in.}}$; this is an indication that precise determination of the threshold stress-intensity factor may not be necessary

---

*The approach taken in the current study was to determine the predicted allowable life using the fatigue crack-growth approach assuming that the largest preexisting flaw allowed by Sect. III was present and compare it with the predicted allowable life using the S-N approach of Sect. III.

for design application. Further analytical studies to determine whether this is generally true and to more fully determine the effect of variations in the threshold stress-intensity factor on calculated lifetimes of a variety of components would help in defining how much effort is justified on precise experimental determination of threshold stress-intensity factors.

6. CONCLUSIONS

This study shows that fatigue failure of the terminal end of the Zion-1 hot-leg piping is extremely unlikely according to both the S-N approach and the fatigue crack-growth approach. The only way to directly compare the two methods is to compare the number of lifetimes that the methods would allow. The fatigue crack-growth approach allows fewer lifetimes of operation than the S-N approach. However, direct comparison of the two approaches is not valid because the design margin included in both procedures is variable and hard to quantify. In the case of the S-N approach, a factor of 2 on stress or 20 on cycles, whichever is the most conservative, is applied to the best-fit curve through the data. This results in a factor on cycles much greater than 20 in the high-cycle regime and a factor on stress greater than 2 in the low-cycle regime. However, tests on prototypic vessels have shown that the actual design margin can be much less.[16] A realistic fatigue crack-growth analysis was performed for one lifetime, but the analysis was not continued for additional lifetimes. If this analysis had been continued for a sufficient number of lifetimes to cause the crack to propagate to failure, it would have provided some indication of the margin included in the Sect. XI procedure. As it is, this margin is unknown.

Until recently, the assumption of the Sect. III fatigue approach (stress ranges less than that which will produce failure in 10^6 cycles need not be considered) was potentially unconservative because very small stress ranges of sufficient frequency can contribute an appreciable amount of fatigue damage. The recent extension of the fatigue design curves for austenitic steels to 10^{11} cycles will help to take care of this problem for austenitic materials. Work is under way to also extend the fatigue design curves for ferritic steels to a higher number of cycles as well.

The existence of a stress-intensity factor threshold was an important assumption in the crack-growth analyses that determines how well this approach treats small stress-range events. Exclusion of a threshold caused extensive or critical crack growth within the 40-year design lifetime. Also, the analytical stress-intensity factor calculations in Appendix A, Sect. XI of the Code do not produce consistent results with the influence function approach in the DRIVE computer program.[33] The Sect. XI approach predicts faster growth on the surface of a part-through crack than at the center, whereas the DRIVE predictions show faster growth at the center relative to the free surface. This inconsistency makes it difficult to exactly quantify the final flaw dimensions and the critical number of 40-year design lifetimes.

The current study is not a sufficient basis for defining any specific changes in either Sect. III or Sect. XI of the Code. However, a number of recent studies[4,45,48,49] have concluded that in certain instances the fatigue crack-growth approach is more conservative than the current Sect. III fatigue evaluation when initial flaws of a reasonable size are assumed. We suggest that it might be prudent to require that the fatigue crack-growth method be applied if the fatigue usage factor is very high. Unfortunately, there is not sufficient information at this time to determine what usage factor, if any, should trigger a requirement for a fatigue

crack-growth analysis. Explicit consideration of the existence of manufacturing defects in the design Code would lead to a more reliable design for areas that actually experience high usage. Furthermore, since the potential manufacturing defect should be related to the method of manufacture and level of inspection and quality control, there would be increased incentive to produce higher quality components where such quality is needed.

One direction that could be taken to improve the Sect. III fatigue design approach would be to require that a fatigue crack-growth analysis be done if the cumulative usage factor is higher than some designated value. The limited study by Anderson et al. suggests that for the problem that they examined and an initial crack depth of 5% of the wall thicknesses, the fatigue crack-growth approach would limit one to a cumulative usage factor of 0.3. However, considerable additional work would be required to determine the value of the cumulative usage factor when the fatigue crack-growth approach predicted failure for a variety of problems before a definite value could be assigned to the designated cumulative usage factor that would trigger a fatigue crack-growth analysis. Such an approach would have minimum impact on the analyst applying the Code because very few locations would ever be expected to have a high enough cumulative usage factor to require the fatigue crack-growth analysis. The "belt and suspenders" approach of requiring that both methods be used in those few critical locations would reduce the possibility of fatigue failure.

Some additional work is needed to establish whether the stress distribution in locations such as nozzles and elbows, where the fatigue usage factors are near 1.0, has an appreciable effect on the number of cycles required to cause a crack to propagate to failure. More importantly, documented fatigue failures in boiling water reactors (BWRs) and PWRs should be used as the basis for comparing the validity of the cumulative usage factor approach and the fatigue crack-growth approach.

This research suggests that the points of criticism of the earlier parametric study (NUREG-0726) concerning its lack of realism in the through-the-wall stress distribution and loading histogram should not have an appreciable effect on the results of that study. The other principal point of criticism that fatigue usage factors are generally much less than 1.0 was verified. However, it is still important that the fatigue design procedures of Sect. III ensure that a permissible flaw could not propagate to failure in the few instances where high fatigue usage factors do occur. This study concludes that additional studies are warranted to establish the need for modification of the current Sect. III fatigue design approach and to establish a basis for such improvements.

REFERENCES

1. *ASME Boiler and Pressure Vessel Code, Section III, Nuclear Power Plant Components, Division 1*, American Society of Mechanical Engineers, New York, 1983.

2. B. F. Langer, "Design of Pressure Vessels for Low-Cycle Fatigue," *J. Basic Eng.* 84(3), 389-402 (September 1962).

3. *ASME Boiler and Pressure Vessel Code, Section XI, Rules for Inservice Inspection of Nuclear Power Plant Components*, American Society of Mechanical Engineers, New York, 1983.

4. W. F. Anderson, G. H. Weidenhamer, and E. C. Johns, *Preliminary Analysis of the Effect of Fatigue Loading and Crack Propagation on Crack Acceptance Criteria for Nuclear Power Plant Components*, NUREG-0726, U.S. Nuclear Regulatory Commission, April 1981.

5. *Pipe Breaks for the LOCA Analysis of the Westinghouse Primary Coolant Loop*, WCAP-8172-A, Westinghouse Electric Corp., January 1975.

6. A. L. Chan, S. C. Lu, E. F. Rybicki, and D. J. Curtis, *Probability of Pipe Fracture in the Primary Coolant Loop of a PWR Plant; Volume 3: Nonseismic Stress Analysis; Load Combination Program; Project I Final Report*, NUREG/CR-2189, vol. 3, UCID-18967, vol. 3, August 1981.

7. S. C. L , S. M. Ma, and R. A. Larder, *Probability of Pipe Fracture in the Primary Coolant Loop of a PWR Plant, Vol. 4: Seismic Response Analysis; Load Combination Program; Project I Final Report*, NUREG/CR-2189, vol. 4, UCID-18967, vol. 4, September 1981.

8. *ASME Boiler and Pressure Vessel Code, Section III*, Article NB-2540 1980.

9. D. O. Harris, E. Y. Lim, and D. D. Dedhia, *Probability of Pipe Fracture in the Primary Coolant Loop of a PWR Plant; Volume 5: Probabilistic Fracture Mechanics Analysis; Load Combination Program; Project I Final Report*, NUREG/CR-2189, vol. 5, UCID-18967, vol. 5, August 1981.

10. M. E. Mayfield et al., *Cold Leg Integrity Evaluation*, NUREG/CR-1319, U.S. Nuclear Regulatory Commission, February 1980.

11. *Criteria of the ASME Boiler and Pressure Vessel Code for Design by Analysis in Sections III and VIII, Division 2*, American Society of Mechanical Engineers, New York, 1969.

12. L. F. Coffin, Jr., et al., "Report of the ASME Boiler and Pressure Vessel Committee, Special Committee to Review Code Stress Basis, Task Group on Fatigue," *Trans. ASME, J. Pressure Vessel Technol.* 100, 240–42 (May 1978).

13. J. Tavernelli and L. F. Coffin, "Experimental Support for Generalized Equation Predicting Low-Cycle Fatigue," *J. Basic Eng., Trans. ASME*, 533–37 (December 1962).

14. S. S. Manson, "Thermal Stresses in Design — Part 19: Cyclic Life of Ductile Materials," *Mach. Des.*, 139 (July 7, 1960).

15. M. J. Manjoine and R. E. Tome, "Proposed Design Criteria for High Cycle Fatigue of Austenitic Stainless Steel," in *ASME International Conference on Advances in Life Prediction Methods*, Albany, New York, April 18–20, 1983, New York, 1983.

16. C. W. Lawton, "High-Temperature Low-Cycle Fatigue: A Summary of Industry and Code Work," *Exp. Mech.*, 257–66 (June 1968).

17. E. C. Rodabaugh and S. E. Moore, *Comparisons of Test Data with Code Methods for Fatigue Evaluation*, ORNL-TM-3520, Union Carbide Corp. Nuclear Div., Oak Ridge Natl. Lab., November 1971.

18. E. Kiss, J. D. Heald, and D. A. Hale, *Low-Cycle Fatigue of Prototype Piping*, GEAP-10135, General Electric (San Jose), January 1970.

19. J. D. Harrison and S. J. Maddox, "Derivation of Design Rules for Pressure Vessels, Avoiding Failure by Fatigue in Welded Constructions," Welding Institute Seminar (October 1979).

20. C. E. Jaske and W. J. O'Donnell, "Fatigue Design Criteria for Pressure Vessel Alloys," *J. Pressure Vessel Technol., Trans. ASME* 99, 584–92, November 1977.

21. Discussion of Ref. 15, *J. Pressure Vessel Technol., Trans. ASME* 100, 236–53, May 1978.

22. *ASME Boiler and Pressure Vessel Code, Section III, Rules for Construction of Nuclear Power Plant Components, Division 1 — Appendices*, American Society of Mechanical Engineers, New York, 1983.

23. M. J. Manjoine and E. I. Landerman, "Techniques for Fatigue Testing and Extrapolation of Fatigue Life for Austenitic Stainless Steels," *J. Test. Eval.*, JTEVA 10(3), 115–20, May 1982.

24. M. A. Miner, "Cumulative Damage in Fatigue," *J. Appl. Mech., Trans. ASME* 67(12), A-159–A-164, September 1945.

25. W. B. Wright and E. C. Rodabaugh, "A Method of Computing Stress Range and Fatigue Damage in a Nuclear Piping System," *Nucl. Eng. Des.* 22, 318–25 (1972).

26. K. H. Liebelt, *Thermal Transients for Fracture Analysis of Zion 1 PWR Primary Loop Hot Leg Piping*, EG&G Idaho, Inc., Internal Technical Report No. RE-A-82-080, December 1982.

27. *ASME Boiler and Pressure Vessel Code, Section III*, Paragraph NB-3650, Analysis of Piping Products (1980).

28. *ASME Boiler and Pressure Vessel Code, Section III*, Appendix I (1980).

29. G. E. Forsythe, M. A. Malcom, and C. B. Moler, *Computer Methods for Mathematical Computations*, Prentice-Hall, Inc., Englewood Cliffs, N.J., 1977.

30. *ASME Boiler and Pressure Vessel Code, Section III*, Paragraph NB-3222, Level A Service Limits, Subparagraph 4e(2), 1980.

31. B. L. Langer, *Application of Stress-Concentration Factors*, Bettis Technical Review, WAPD-BT-18, April 1960.

32. R. R. Maccary, *Nondestructive Examination Acceptance Standards, Technical Basis and Development of Boiler and Pressure Vessel Code, ASME Section XI, Division 1*, EPRI NP-1406-SR, May 1980.

33. D. Dedhia and D. O. Harris, *Stress Intensity Factors for Surface Cracks in Pipes: A Computer Code for Evaluation by Use of Influence Functions*, EPRI NP-2425, June 1982.

34. E. K. Walker, "An Effective Strain Concept for Crack Propagation and Fatigue Life with Specific Applications to Biaxial Stress Fatigue," *Proc. Air Force Conf. Fatigue and Fracture of Aircraft Structures and Materials*, Miami Beach, Fla, December 15–18, 1969.

35. P. Rabbé and H. P. Lieurade, "Etude a l'Aide de la Mecanique de la Rupture de la Vitesse de Fissuration en Fatigue d'une Gamme Entendue d'Aciers," *Memoires Scientifiques, Rev. Metallurgie, LXIX*, No. 9, September 1972.

36. Data base for Environmental Crack Model Development, maintained for EPRI by Battelle-Columbus Laboratories.

37. L. A. James, "Fatigue-Crack Growth Correlations for Design and Analysis of Stainless Steel Components," Pressure Vessel and Piping Division of the ASME, 82-PVP-25.

38. L. A. James, "Fatigue-Crack Propagation in Austenitic Stainless Steels," *At. Energy Rev.* 14(1), 37–86 (1976).

39. L. A. James, "The Effect of Elevated Temperature Upon the Fatigue-Crack Propagation Behavior of Two Austenitic Stainless Steels," *International Conference on Mechanical Behavior of Materials, 1st Kyoto, 1971 Proceedings*, 3, 1972, pp. 341–52.

40. P. Shahinian, H. Smith, and J. Hawthorne, "Fatigue Crack Propagation in Stainless Steel Weldments at High Temperature," *Welding Research Supplement*, 527–32 (1972).

41. W. Bamford, "Fatigue Crack Growth of Stainless Steel Piping in a Pressurized Water Reactor Environment," *J. Pressure Vessel Technol.* 101, 73–79 (1979).

42. A. Pickard, R. Ritchie, and J. F. Knott, "Fatigue Crack Propagation in a Type 316 Stainless Steel Weldment," *Met. Technol.* 2, 253–63 (1975).

43. B. L. Harris, letter to W. L. Server, BLH-15-82, "Stress Analysis of Primary Coolant Loop Piping for Thermal Transients in a PWR Plant," December 14, 1982.

44. *ASME Boiler and Pressure Vessel Code, Section XI*, Non-Mandatory Appendix C, "Evaluation of Flaws in Austenitic Piping," Passed by Main Committee on 5/5/83 also to appear in the Winter 1983 Addenda to Section XI.

45. F. A. Simonen and C. W. Goodrich, *Parametric Calculations of Fatigue Crack Growth in Piping*, NUREG/CR-3059, PNL-4537, R5, March 1983.

46. J. J. Hamn, J. E. Roberts, J. C. Lowry, and R. W. Burge, *Analytical Report for Florida Power and Light Company, St. Lucie Plant Unit No. 2 Piping*, CENC-1501, Combustion Engineering, Inc., February 1982.

47. K. Kussmaul, "Developments in Nuclear Pressure Vessel and Circuit Technology in the Federal Republic of Germany," pp. 1–28 in *Structural Integrity of Light Water Reactor Components*, ed. L. E. Steele et al., Applied Sciences Publishers, 1981.

48. P. M. Scott, B. Tomkins, and A. J. E. Foreman, "Development of Engineering Codes of Practice for Corrosion Fatigue," ASME Paper No. 82-PVP-30 (June 1982); also *J. of Pressure Vessel Technol., Trans. ASME* 105(3), 255–62 August 1983.

49. Letter, Carl E. Jaske, Battelle, to James A. Horak, Oak Ridge National Laboratory, private communication (February 26, 1982).

NUREG/CR-3982
ORNL-6099
Dist. Category RM

Internal Distribution

1. C. R. Brinkman
2. J. J. Blass
3. S. J. Chang
4. J. A. Clinard
5. C. W. Collins
6. J. M. Corum
7. D. M. Eissenberg
8. W. L. Greenstreet
9. D. S. Griffith
10-14. R. C. Gwaltney
15. W. R. Hendrich
16. R. L. Huddleston
17. Y. L. Lin
18. A. P. Malinauskas
19. S. S. Manson (Consultant)
20. J. G. Merkle
21. S. E. Moore
22. D. G. O'Conner
23. C. E. Pugh
24. H. E. Trammell
25. G. D. Whitman
26-30. G. T. Yahr
31. ORNL Patent Office
32. Central Research Library
33. Document Reference Section
34-35. Laboratory Records Department
36. Laboratory Records (RC)

External Distribution

37. Office of Assistant Manager for Energy Research and Development, Department of Energy, ORO, Oak Ridge, TN 37831
38-39. Technical Information Center, DOE, Oak Ridge, TN 37831
40-44. A. K. Richardson, EG&G Idaho, Inc., P.O. Box 1625, Idaho Falls, Idaho 83415
45-49. W. L. Server, EG&G Idaho, Inc., P.O. Box 1625, Idaho Falls, Idaho 83415
50-349. Given distribution as shown under category RM (NTIS-10)
350-412. Special ASME Code Distribution (by NRC)

NRC FORM 335 (2.84) NRCM 1102, 3201, 3202

U.S. NUCLEAR REGULATORY COMMISSION

BIBLIOGRAPHIC DATA SHEET

SEE INSTRUCTIONS ON THE REVERSE

1 REPORT NUMBER (Assigned by TIDC, add Vol. No., if any)
NUREG/CR-3982
ORNL-6099

2 TITLE AND SUBTITLE
Case Study of the Propagation of a Small Flaw Under PWR Loading Conditions and Comparison with the ASME Code Design Life — Comparison of ASME Code Sections III and XI

3 LEAVE BLANK

4 DATE REPORT COMPLETED
MONTH: October
YEAR: 1984

5 AUTHOR(S)
G. T. Yahr
A. K. Richardson*
R. C. Gwaltney
W. L. Server*
*EG&G Idaho, Inc.
Idaho Falls, ID 83415

6 DATE REPORT ISSUED
MONTH: November
YEAR: 1984

7 PERFORMING ORGANIZATION NAME AND MAILING ADDRESS (Include Zip Code)
Oak Ridge National Laboratory
P.O. Box Y
Oak Ridge, TN 37831
EG&G Idaho, Inc.
Idaho Falls, ID 83415

8 PROJECT/TASK/WORK UNIT NUMBER

9 FIN OR GRANT NUMBER
B0474
A6367

10 SPONSORING ORGANIZATION NAME AND MAILING ADDRESS (Include Zip Code)
Division of Engineering Technology
Office of Nuclear Regulatory Research
U.S. Nuclear Regulatory Commission
Washington, DC 20555

11a TYPE OF REPORT
Topical

b PERIOD COVERED (Inclusive dates)

12 SUPPLEMENTARY NOTES

13 ABSTRACT (200 words or less)

A cooperative study was performed by EG&G Idaho, Inc. and Oak Ridge National Laboratory to investigate the degree of conservatism and consistency in the *ASME Boiler and Pressure Vessel Code* Sect. III fatigue evaluation procedure and Sect. XI flaw acceptance standards. A single, realistic, sample problem was analyzed to determine the significance of certain points of criticism of an earlier parametric study by staff members of the Division of Engineering Standards of the Nuclear Regulatory Commission. The problem was based on a semielliptical flaw located on the inside surface of the hot-leg piping at the reactor vessel safe-end weld for the Zion 1 pressurized-water reactor (PWR). Two main criteria were used in selecting the problem: first, it should be a straight pipe to minimize the computational expense; second, it should exhibit as high a cumulative usage factor as possible. Although the problem selected has one of the highest cumulative usage factors of any straight pipe in the primary system of PWRs, it is still very low.

The Code Sect. III fatigue usage factor was only 0.00046, assuming it was in the as-welded condition, and fatigue crack-growth analyses predicted negligible crack growth during the 40-year design life. When the analyses were extended past the design life, the usage factor was less than 1.0 when the flaw had propagated to failure. The current study shows that the criticism of the earlier report should not detract from the conclusion that if a component experiences a high level of cyclic stress corresponding to a fatigue usage factor near 1.0, very small cracks can propagate to unacceptable sizes.

14 DOCUMENT ANALYSIS — a. KEYWORDS/DESCRIPTORS

b. IDENTIFIERS/OPEN-ENDED TERMS

15 AVAILABILITY STATEMENT
Unlimited

16 SECURITY CLASSIFICATION
(This page) Unclassified
(This report) Unclassified

17 NUMBER OF PAGES

18 PRICE

120555078877 1 1ANIRM
US NRC
ADM-DIV OF TIDC
POLICY & PUB MGT BR-PDR NUREG
W-501
WASHINGTON DC 20555